Battery-Less Wireless Instrumented Tibial Tray

A THESIS
SUBMITTED TO THE FACULTY OF THE GRADUATE SCHOOL
OF THE UNIVERSITY OF MINNESOTA
BY

James Holmberg

IN PARTIAL FULFILLMENT OF THE REQUIREMENTS
FOR THE DEGREE OF
Master of Science

Advisor: Professor Rajesh Rajamani

November, 2011

Acknowledgements

I would like to thank my advisor, Professor Rajesh Rajamani, for the opportunity to work on this project and for his continuous support and patience. I would also like to thank Lee Alexander for his support, assistance, and for his hard work machining all of the mechanical prototype parts for this project. Professor Joan Bechtold was also very helpful as she provided useful background information for this project and also insightful feedback on concepts. Last but not least, I would like to thank my wife, Desiree Holmberg, for her love, patience, and understanding, and my parents, Dave and Kathy Holmberg, for their support and encouragement.

Abstract

Previous research has found that over 400,000 total knee replacement procedures (TKR) are annually performed in the United States. Therefore, it is important that the loads on TKR implants be fully understood to improve the reliability of the implants. This paper presents the development of a battery-less wireless instrumented tibial tray for TKR implants. Previous instrumented tibial trays were powered by inductive coupling which required the patient to wear an externally-powered coil. Whereas, the proposed instrumented tibial tray is powered internally by an integrated piezoelectric energy harvesting system. This paper also presents the development of capacitive force sensors and an ultra low-power method to measure the capacitive force sensors. Two capacitive force sensor designs were considered and neither design could meet all of the performance requirements for the intended application. Despite this finding, several sensors were produced to demonstrate the concept behind capacitive force sensing using piezoelectric energy harvesting. With a 316 lb applied force, the energy harvesting system could fully charge the storage capacitors in 11 steps and could harvest an average of 1051 μJ per step. To power the force measurement system for ten seconds and to transmit the data, the piezoelectric energy harvesting system must be charged before the force measurement process is initiated by a minimum of 11 steps with a force of 316 lbs and a minimum of two steps must be taken during the force measurement process. During the force measurement process, each force sensor was sampled at a frequency of 10 Hz for 10 seconds; thereafter, all of the data was transmitted to the RF base station. The resulting capacitive force sensors showed good results when a set of cyclic loads were applied; however, the sensors demonstrated issues with repeatability when the applied force was increased and then reduced to the original value. The force sensors require improvements, but once this is completed, the system shows promise to be an effective measurement device for TKR implants.

Table of Contents

Acknowledgements i

Abstract ii

Table of Contents iii

List of Tables vi

List of Figures vii

Chapter 1 – Introduction 1

1.1 Overview 1

1.2 Motivation for Battery-Less Wireless Instrumented Tibial Tray 1

1.3 Current Approaches 2

1.4 Thesis Contributions 4

1.5 Organization of Thesis 4

Chapter 2 – The Knee 6

2.1 Anatomy of the Knee 6

2.2 Forces in the Knee 6

2.3 Overview of Total Knee Replacement Surgery 7

Chapter 3 – Energy Harvesting 8

3.1 Introduction 8

3.2 Piezoelectric Energy Harvesting 8

3.2.1 Piezoelectric Transducer 11

3.2.2 Improving the Performance of Piezoelectric Energy Harvesting 12

Chapter 4 – Load Sensing 15

4.1 Introduction 15

4.1.1 Load Cells and Strain Gages 15

4.1.2 Piezoresistive sensors 15

4.1.3 Capacitive sensors 16

4.2 Measurement of Capacitance 16

4.2.1 RC Time Constant Method 17
4.3 Design of Capacitive Sensors 23
4.3.1 Introduction 23
4.3.2 Design Constraints and Performance Requirements 23
4.3.3 Sensor Concept # 1 – Allow force to change area of capacitor 24
4.3.4 Sensor Concept # 2 – Allow force to change dielectric thickness 27
4.4 Arrangement of Sensors 31
Chapter 5 – Wireless Data Transmission 33
5.1 Introduction 33
5.2 Hardware and Electrical Design 33
5.3 Software Configuration 34
Chapter 6 – Experimental Setup 36
6.1 Introduction 36
6.2 Design of Tibial Component 36
6.3 Capacitive Force Sensors 38
6.4 Gait Simulator 38
Chapter 7 – Results 42
7.1 Introduction 42
7.2 Piezoelectric Energy Harvesting 42
7.3 Capacitive Force Sensing 46
7.3.1 Relationship between Discharge Time and Capacitance 47
7.3.2 Relationship between Capacitance and Force 48
7.4 System Power Consumption 54
7.4.1 Power Consumption while Measuring Sensors 55
7.4.2 Power Consumption while Transmitting Data 56
Chapter 8 – Conclusions and Future Research 58
8.1 Summary and Conclusions 58
8.2 Future Research 59
Works Cited 61

Appendix A 64

Appendix B 66

List of Tables

Table 1 – Design Parameters for Concept # 1 25
Table 2 – Design Parameters for Concept # 2 28
Table 3 – Calculated loads for gait simulator 40
Table 4 – Performance of Piezoelectric Energy Harvesting Power Supply 43
Table 5 – Calculated Stray Capacitance for Each Measurement Circuit..... 49

List of Figures

Figure 1 – Total knee replacement implant instrumented for in vivo force and moment measurements 3
Figure 2 – Forces within knee measured in-vivo for level ground walking 4
Figure 3 – Anatomy of Knee 6
Figure 4 – Total knee replacement implant 7
Figure 5 – Layout of instrumented tibial tray 9
Figure 6 – Equivalent Circuit Model of Piezoelectric Transducer 9
Figure 7 – Schematic of Typical PEHS Circuit 10
Figure 8 – Output voltage of piezoelectric stack 11
Figure 9 – State diagram of energy harvesting system 13
Figure 10 – Schematic for RC time constant measurement circuit 17
Figure 11 – Flowchart of Capacitance Measurement 20
Figure 12 – Diagram of concept # 1 for a capacitive sensor 25
Figure 13 – Diagram of concept # 2 for a capacitive sensor 28
Figure 14 – Graph showing non-linear relationship 29
Figure 15 –Arrangement of Force Sensors in Tibial Component 31
Figure 16 – Picture of final knee implant from Pro-Engineer 37
Figure 17 – Cross-section of final knee implant showing layout of various components 37
Figure 18 – Final design of capacitive force sensor 38
Figure 19 – Picture of Gait Simulator 39
Figure 20 – Typical loading cycle with gait simulator at 40 psi air pressure 41
Figure 21 – Typical charging cycle for 188 lbs nominal peak force 42
Figure 22 – Relationship between harvested energy of PEHS and applied force 44
Figure 23 – The top graph shows the force linearly increasing on the piezo transducer. The middle graph shows the voltage on the input capacitor which is coupled to the piezo transducer by a full-wave rectifier. The bottom graph shows the voltage on the storage capacitor. 45
Figure 24 – State Diagram for Capacitive Sensor Measurements 46
Figure 25 – Relationship between discharge time and capacitance 47

Figure 26 – Charge / discharge cycle for capacitance measurement 48
Figure 27 – Layout of capacitive sensors in gait simulator 49
Figure 28 – Relationship between measured sensor capacitance and force. Important note: The load cell measured the total force applied to all of the sensors. This force was divided by six to obtain the force applied to each individual sensor. 50
Figure 29 - Layout of capacitive sensors in gait simulator when rotated 180° 51
Figure 30 – Force measurements for sensor # 1, after calibration completed 52
Figure 31 – Force measurements for sensor # 2, after calibration completed 52
Figure 32 – Force measurements for sensor # 3, after calibration completed 53
Figure 33 – Force measurements for sensor # 4, after calibration completed 53
Figure 34 – Force measurements for sensor # 5, after calibration completed 54
Figure 35 – Force measurements for sensor # 6, after calibration completed 54
Figure 36 – Storage capacitor voltage while measuring Sensors at 10 Hz 55
Figure 37 – Storage capacitor voltage while transmitting data 57
Figure 38 – Page 1 of schematic for electrical circuit 64
Figure 39 – Page 2 of schematic for electrical circuit 65
Figure 40 – Front view of final device 66
Figure 41 – Side view of final device 66
Figure 42 – Picture showing circuit board, ground plate, and compliant material for sensors 67

Chapter 1 – Introduction

1.1 Overview

This thesis investigates a battery-less wireless force sensor integrated into a tibial tray as part of a total knee replacement (TKR). The basic objective of a TKR procedure is to replace the load-bearing surfaces of the knee joint with a knee replacement implant. Integrating force sensors into the knee implant can be beneficial for several reasons as will be discussed in the following section. Wireless data transmission and a battery-less design allow the system to be autonomous within the patient, only requiring an external receiver to obtain the measurement data.

1.2 Motivation for Battery-Less Wireless Instrumented Tibial Tray

According to a report by (Kurtz, Ong, Edmund, Mowat, & Halpern, 2007), in 2003 the number of TKR's performed annually in the United States had exceeded 400,000. Further research has shown that the failure rate of knee replacements is approximately 10% after ten years and 20% after 20 years (NIH Consensus Development Conference on Total Knee Replacement, 2003). Due to the complexity, cost, and rehabilitation time for TKR procedures, it is imperative that the reliability of the TKR implant be significantly improved. Furthermore, TKRs are occasionally performed on patients less than 50 years of age, for which an implant lifetime of 10 to 20 years is inadequate. Revision surguries to replace the original knee replacement are more technically challenging, and correspondingly risky, than the original surgery (Ong, Lau, Suggs, Kurtz, & Manley, 2010). Thus, importance should be placed on improving the reliability of the TKR implant to decrease the number of implant failures and to correspondingly decrease the number of revision surgeries.

The primary failure modes for TKR implants are infection (25%), implant loosening (16%), and implant failure (10%) (Bozic, et al., 2010). This thesis attempts to produce an instrumented tibial tray that can identify implant misalignment, implant failure, and component wear. It is believed that these objectives could be accomplished by initially

measuring the force distribution across the knee and then obtaining the same set of measurements at future points in time. The initial force distribution would be used to serve as a baseline for future comparisons. By periodically measuring the force distribution across the knee, this information could be used to verify that the implant does not move or wear during the life of the implant.

Another potential use of an implanted tibial tray is for soft-tissue balancing. Currently, a "balanced" knee is subjective and depends on the particular surgeon performing the procedure. Various technologies have been developed to make soft-tissue balancing more objective, but these methods have not been widely implemented. An instrumented tibial tray could provide direct feedback to the surgeon as to whether the knee was properly balanced throughout the entire flexion range.

The final proposed use of an instrumented tibial tray includes measurement of activity level. For example, the force measurements could be used to simultaneously measure the amplitude of the loads in the knee and to count the number of steps walked by a patient in a given time period. This information could help both the patient and physician to understand if the activity level of the patient matches the recommended rehabilitation procedure, and also to determine if the activity level or rehabilitation procedure needs to be modified.

1.3 Current Approaches

There are several systems in existence today that measure knee loads in vivo (D'Lima, Townsend, Arms, Morris, & Jr, 2005) and (Heinlein, Graichen, Bender, Rohlmann, & Bergmann, 2007). A picture of the device used by (Kutzner, et al., 2010) is shown below in Figure 1.

Figure 1 – Total knee replacement implant instrumented for in vivo force and moment measurements

The system originally presented by (Heinlein, Graichen, Bender, Rohlmann, & Bergmann, 2007) included six strain gages on the tibial shaft and was capable of measuring all six force and moment components in-vivo. Data from this system was presented in (Heinlein, et al., 2009) and (Kutzner, et al., 2010) and has shown to be very effective at measuring loads for a variety of activities. Figure 2 below is courtesy of (Orthoload, 2011) and shows the measured forces for a level-ground gait cycle.

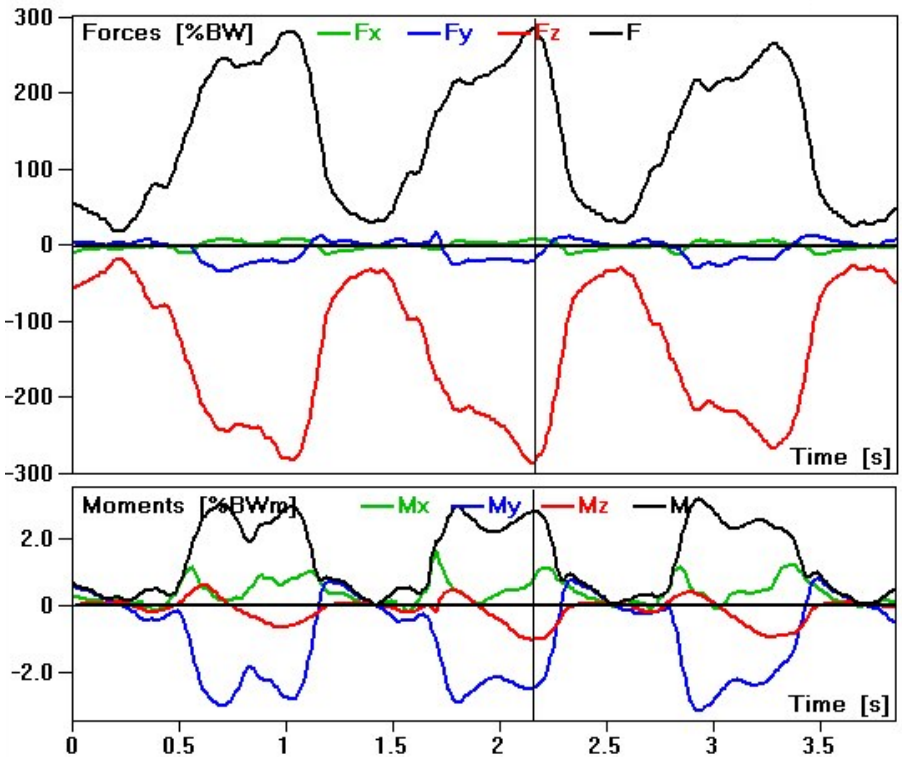

Figure 2 – Forces within knee measured in-vivo for level ground walking

One limitation of these systems is that they are dependent on an external power supply to allow them to operate. The primary method for powering the devices has been inductive coupling, which uses an AC voltage source to power an external coil placed in close proximity to the implanted device. This requirement for external power makes these systems impractical for acquiring data outside of the laboratory or doctor's clinic.

1.4 Thesis Contributions

The novel contribution from this thesis was to integrate energy harvesting into an instrumented tibial tray for knee replacement implants. As described earlier, load sensing within the knee is not a novel idea, but the capacitive-type force sensor that was developed may be a first for this application.

1.5 Organization of Thesis

This thesis is organized as follows: Chapter 2 discusses the anatomy of the knee and TKR procedures, Chapter 3 discusses the development of an energy harvesting system,

Chapter 4 discusses the design of a load sensing system, Chapter 5 discusses wireless data transmission, Chapter 6 discusses the experimental setup and the specific equipment needed to perform testing, Chapter 7 presents the data from all of the testing that was completed, and Chapter 8 discusses the results from Chapter 7 and presents conclusions and suggestions for future work.

Chapter 2 – The Knee

2.1 Anatomy of the Knee

The anatomy of the knee can best be presented and explained with Figure 3 below (ACL Solutions). The important observations are the locations of the femur and tibia and the approximate geometry of these bones.

Figure 3 – Anatomy of Knee

2.2 Forces in the Knee

There has been a considerable amount of research on calculating and measuring the forces within the knee. Several different approaches have been taken, such as theoretical calculations (Morrison, 1970), computational finite element analysis (Godest, Beaugonin, Haug, Taylor, & Gregson, 2002), and direct measurement with implanted sensors (Mündermann, Dyrby, D'Lima, Colwell, & Andriacchi, 2008) and (Bozic, et al., 2010). According to (Bozic, et al., 2010), where forces were measured with implanted sensors, average peak loads on a knee joint were 264% of body weight during level walking. A typical load profile for level walking was shown in Figure 2. The activity that produced the largest load was ascending stairs, where the average peak load was measured at 346% of body weight.

2.3 Overview of Total Knee Replacement Surgery

The TKR procedure can briefly be described by the following process steps. First, the tibia and femur bones are precisely cut to conform to the implant components. Second, the tibial and femoral implant components are attached with cement to the corresponding bones. Between the tibial and femoral components is a polymer insert that serves as the new bearing surface for the knee. The final step is to balance the ligament tension acting on the knee joint; this is accomplished by soft-tissue release. Figure 4 shows a knee replacement implant after the procedure has been completed (Hospital for Special Surgery Website, HSS.edu, 2010).

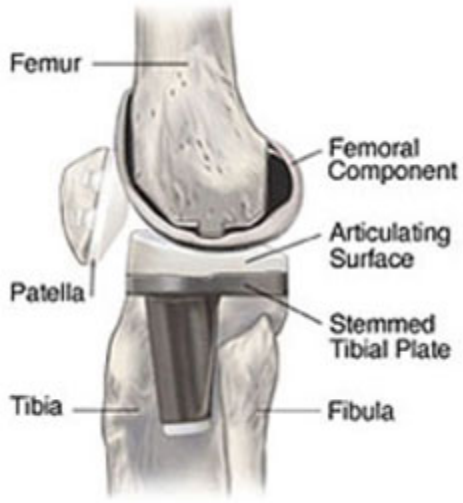

Figure 4 – Total knee replacement implant

The load sensing system presented in this paper is intended to replace the tibial component and the polymer bearing surface. If the polymer bearing surface is properly designed, the system could be fully compatible with existing femoral components.

Chapter 3 – Energy Harvesting

3.1 Introduction

Energy harvesting is a growing set of technologies popularized by both academia and industry. The interest in energy harvesting stems from powering electronics where other external power sources cannot meet the necessary size and performance requirements. There are many energy harvesting technologies in existence today, such as piezoelectric, thermoelectric, and solar power. The energy harvesting technology for this orthopedic application should have a compact package size, provide sufficient power output to meet the application requirement, and be commercially available. Piezoelectric energy harvesting is an established technology that meets all of the above requirements.

3.2 Piezoelectric Energy Harvesting

Piezoelectric energy harvesting systems (PEHS) use the piezoelectric effect, existent in some crystalline materials, to convert mechanical strain energy into electrical energy. PEHS are capable of harvesting energy from a wide range of loading conditions: from vibration type loads to low-frequency, high-force loads. As described in chapter 2, the PEHS for this orthopedic application will be subjected to low-frequency, high-force loading conditions. Basic piezoelectric analysis can show that for single-axis compression loads, the output voltage of the piezoelectric transducer is proportional to strain (Piezo Systems Inc). Consequently, the load on the piezoelectric transducer should be maximized to maximize the amount of energy harvested. To maximize the load applied to the piezoelectric transducer, the transducer should be located such that the weight-bearing forces in the knee are entirely transferred through the transducer. Figure 5 shows the proposed location of the piezoelectric transducer in the knee.

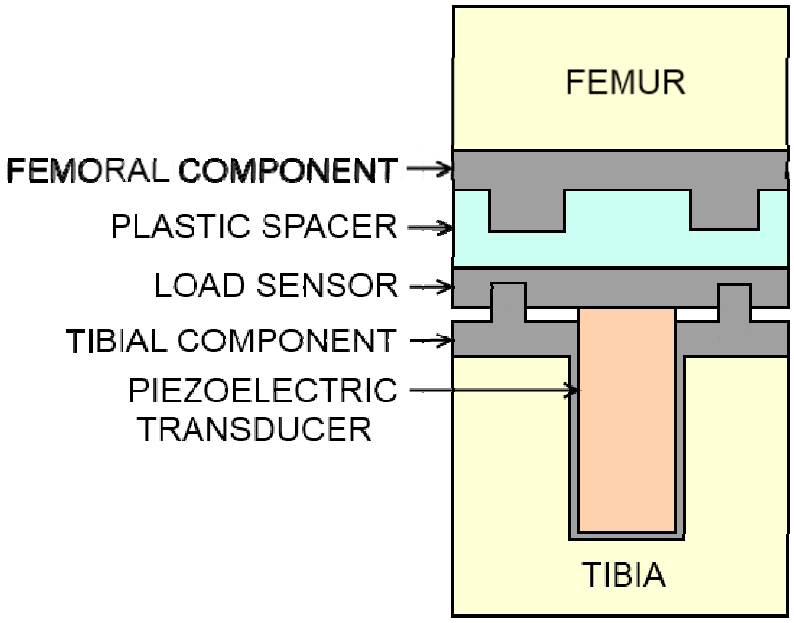

Figure 5 – Layout of instrumented tibial tray

For a theoretical analysis, the piezoelectric transducer can be modeled as a voltage source in series with a capacitor, as shown below in Figure 6 (Park, 2001).

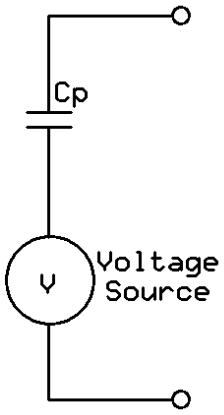

Figure 6 – Equivalent Circuit Model of Piezoelectric Transducer

PEHS typically rectify the output voltage of the piezoelectric transducer and then store energy on a storage capacitor, C_s. Research by (Guan & Liao, 2007) showed that super-capacitors were a better match for piezoelectric energy harvesting than rechargeable batteries, due to their charge/discharge efficiency. A schematic showing a typical PEHS circuit is shown below in Figure 7. Typically, the process works as follows: when the

storage capacitor is adequately charged, the switch is closed and the load, shown here as a resistor, is powered by the storage capacitor.

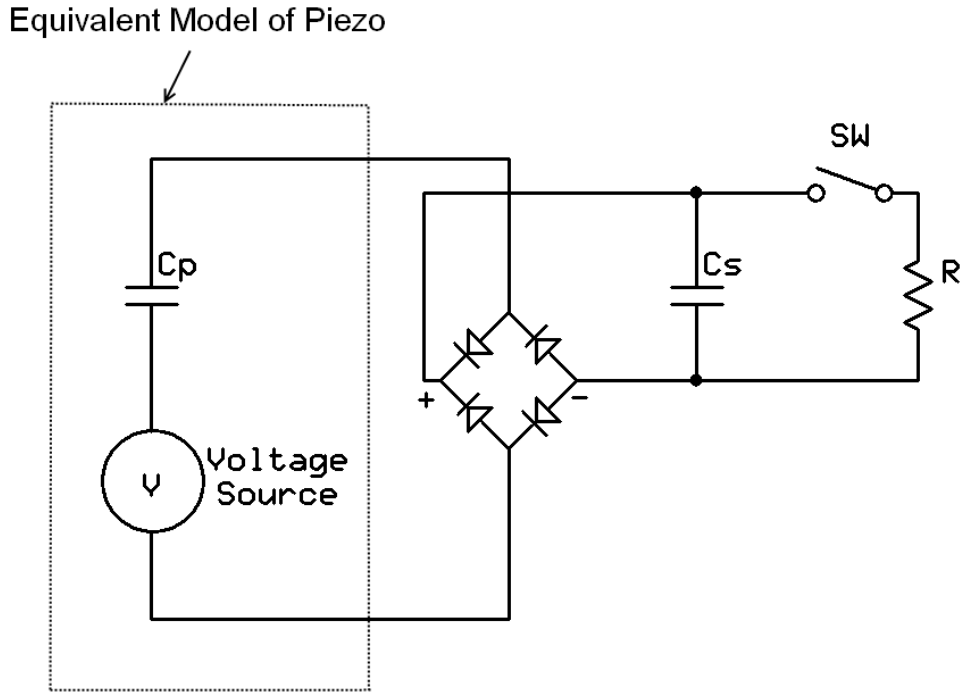

Figure 7 – Schematic of Typical PEHS Circuit

For a given open-circuit voltage on the piezoelectric transducer, the voltage on C_s depends greatly on the capacitance of C_s and C_p. The rectifier will be ignored for the following analysis, because the rectifier effectively provides a fixed voltage drop between the transducer and the storage capacitor. The switch and resistor will also be ignored from this analysis because they do not factor into charging the storage capacitor. Using basic circuit analysis techniques, the following equation can be developed that relates the storage capacitor voltage to the piezo voltage.

$$V_s = V \cdot \frac{C_p}{(C_s + C_p)}$$

The stored energy on the storage capacitor can be calculated as follows.

$$U = \frac{1}{2} \cdot C_s \cdot V_s^2 = \frac{1}{2} \cdot C_s \cdot \left(V \cdot \frac{C_p}{(C_s + C_p)} \right)^2$$

Taking the derivative of the above equation with respect to C_s and setting equal to zero, shows that the maximum storage energy occurs when C_s equals C_p, as shown below.

$$\frac{\partial U}{\partial C_s} = \frac{V^2 \cdot {C_p}^2 \cdot \left(\frac{1}{2} \cdot C_p - \frac{1}{2} \cdot C_s\right)}{\left(C_p + C_s\right)^3}$$

This result will become important later when a circuit must be developed to harvest energy from a piezoelectric transducer.

3.2.1 *Piezoelectric Transducer*

A commercially available piezoelectric transducer intended for compression type loads is the TS18-H5-104 piezoelectric stack (hereafter called "piezo stack") from Piezo Systems Inc. of Woburn, MA. The piezo stack is constructed by stacking 104 layers of 5 mm x 5 mm piezoelectric ceramic into a single package with outer dimensions of 6 mm x 6 mm x 18 mm. This construction places 104 piezoelectric transducers in parallel to maximize the performance and capacitance of the transducer. To determine the performance of the piezo stack, the output voltage was measured for a range of input forces and the results are shown in Figure 8 below.

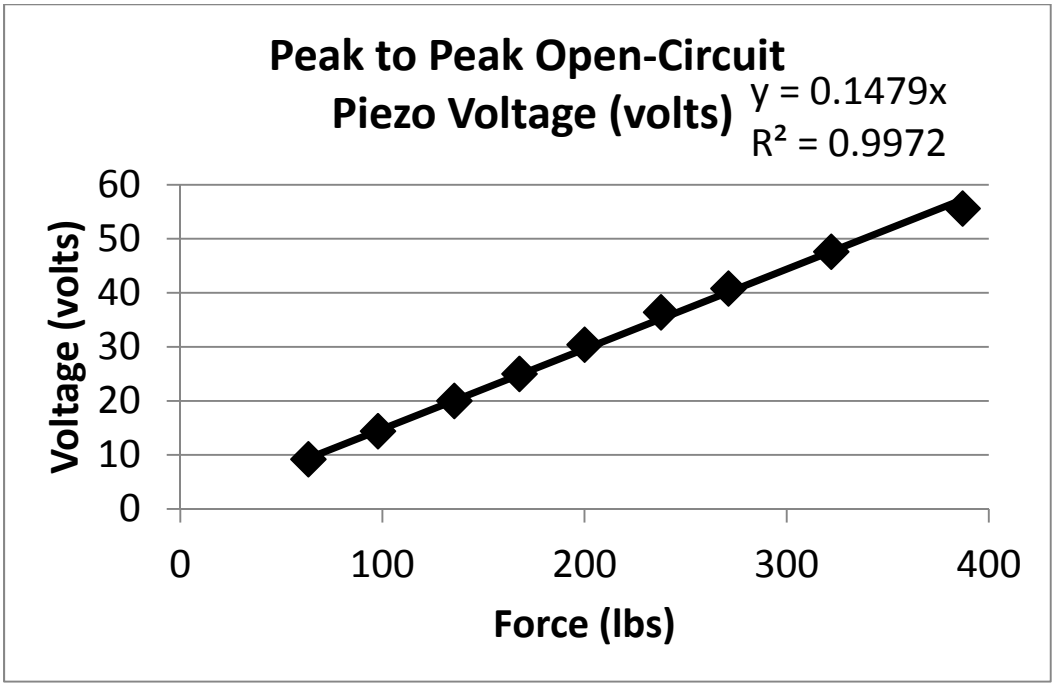

Figure 8 – Output voltage of piezoelectric stack

The results from Figure 8 show a linear relationship between input force and output voltage, which matches the referenced theoretical analysis from section 3.1.

3.2.2 *Improving the Performance of Piezoelectric Energy Harvesting*

There have been many researchers who have presented methods to maximize energy harvesting with piezoelectric materials (Ottman, Hofmann, Bhatt, & Lesieutre, 2002), (Tabesh & Frechette, 2010), and (Vijayaraghavan & Rajamani, 2010). These papers showed that adaptive electrical circuits are necessary for optimal performance.

(Ottman, Hofmann, Bhatt, & Lesieutre, 2002) presented a system that used a DC-DC buck converter with adaptive control on the duty cycle to maximize the current into the battery. Their analysis assumed that the battery voltage changed slowly over time and that maximizing power input into the battery was equivalent to maximizing the current into the battery. However, the system proposed in this paper will use a super-capacitor as a storage device and due to the much smaller storage capacity relative to a battery, the previous assumption does not apply in this case. Consequently, adaptive control of a DC-DC converter is much more difficult to implement for this orthopedic application. (Vijayaraghavan & Rajamani, 2010) presented three different methods for improving piezoelectric energy harvesting: (1) fixed threshold switching, (2) max voltage switching, and (3) switched inductor, which had the best performance.

By combining a DC-DC converter with the fixed-threshold method, a sub-optimal, but potentially acceptable solution can be realized. A commercially available product intended for piezoelectric energy harvesting is the LTC3588 from Linear Technologies. The LTC3588 is available in a small package size, 3 mm x 3 mm x 1.5 mm, yet has a built-in full-wave rectifier on the input and a voltage regulator on the output. The LTC3588 operates by coupling a storage capacitor, C_{in}, to the piezo stack through the full-wave rectifier. When the voltage on C_{in} exceeds a given threshold, the integrated DC-DC buck converter transfers charge from C_{in} to a storage capacitor on the output, C_s. Hysteresis on the threshold voltage for the buck converter prevents the buck converter from oscillating between the active and inactive modes. When C_s is at the set point

voltage, C_{in} will charge up to 20 volts before a shunt is activated to limit the capacitor voltage. Charging C_{in} to a high voltage allows extra energy to be stored by the system and allows C_{in} to serve as a backup to C_s. Figure 9 below shows a state diagram of the energy harvesting process that was previously described.

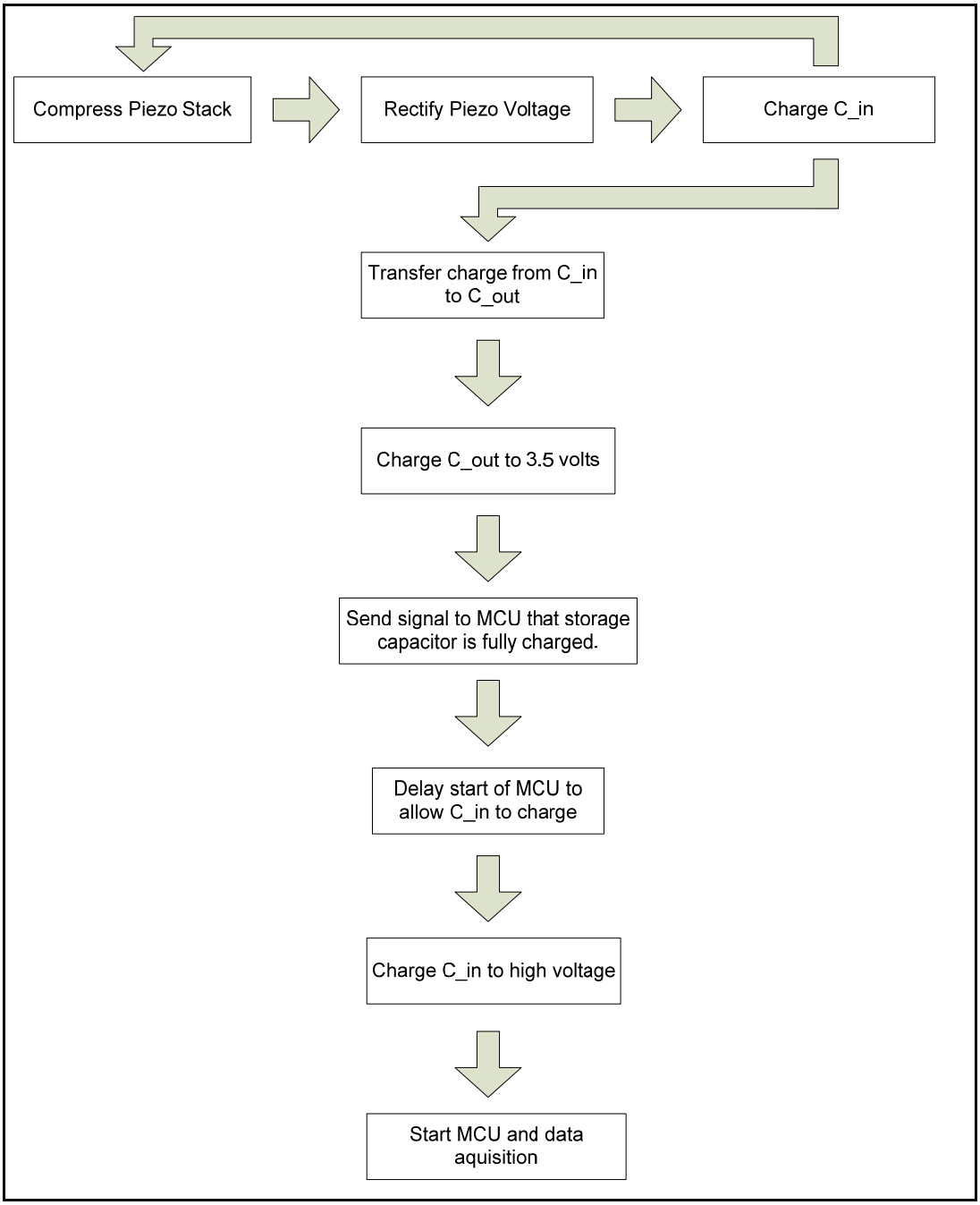

Figure 9 – State diagram of energy harvesting system

The LTC3588 has a status output pin which is intended to alert a microcontroller when the storage device has reached the desired output voltage. This feature of the LTC3588 allows the microcontroller to know the approximate voltage of the storage device and to delay the start of data acquisition until C_{in} has charged to a voltage significantly higher than the primary storage device to allow C_{in} to serve as a backup to the primary storage device.

Chapter 4 – Load Sensing

4.1 Introduction

The engineering community has developed methods to measure loads in a wide variety of applications. For this orthopedic application, there exist a set of constraints that the proposed sensor must meet to produce acceptable results. The three primary constraints are related to the sensor performance, physical size of the sensor, and the size and complexity of the equipment necessary to measure the sensor. The sensor performance will be characterized by many different criteria such as the measurement resolution, measurement range, and measurement accuracy. Several potential load sensing technologies will be briefly discussed below.

4.1.1 *Load Cells and Strain Gages*

Load cells and strain gages have been successfully used in several systems for knee replacement implants (Kaufman, Kovacevic, Irby, & Colwell, 1996) and (Heinlein, Graichen, Bender, Rohlmann, & Bergmann, 2007). The report from (Kaufman, Kovacevic, Irby, & Colwell, 1996) demonstrated that load cells provided accurate measurements of force, but the overall size of the load cells made it difficult to fit them within the boundaries of the implant. The strain gage arrangement presented in (Heinlein, Graichen, Bender, Rohlmann, & Bergmann, 2007) fit well within the implant boundary and had the added ability to output the six load components acting on the implant. Unfortunately, the strain gages in this system were placed on the stem of the tibial tray which would interfere with the proposed location of the piezo stack as shown in Figure 5. Consequently, a new type of sensor technology will be examined to determine if it can meet the constraints previously discussed.

4.1.2 *Piezoresistive sensors*

The piezoresistive effect causes the resistance of a semiconductor to change with respect to applied strain, similar to a typical strain gage or load cell. This type of sensor has become increasingly popular in pressure sensors, accelerometers, and load cells due to their small size and high sensitivity. Unfortunately, a commercially available

piezoresistive sensor could not be found that met the necessary size, shape, and load capacity constraints of this project. Due to their semiconductor nature, piezoresistive sensors are expensive to produce in small quantities, which made custom piezoresistive sensors out of reach for this project. However, for future developments, this type of sensor may be potentially viable for instrumented tibial trays.

4.1.3 *Capacitive sensors*

Capacitive sensors have long been used in proximity sensors, distance sensors, and pressure sensors. The capacitance of a parallel plate capacitor is calculated by the following equation, where ε_0 is the vacuum permittivity, k is the dielectric strength of the material between the plates, A is the overlapping area of the two parallel plates, and t is the distance between the plates.

$$C = \frac{\varepsilon_0 \cdot k \cdot A}{t}$$

Capacitive sensors operate by allowing either k, A, or t to change with respect to the variable of interest. There exist many different methods for which the capacitance of a sensor could change with applied force. However, substantial development will be needed to develop a capacitive sensor that meets the size and performance constraints of this application. Aside from designing the capacitive sensor, a method to measure the capacitance will also be developed.

4.2 Measurement of Capacitance

Several methods exist for measuring capacitance, such as measuring the RC time constant, measuring the AC impedance, or sigma-delta capacitance-to-digital conversion. These three methods have varying capabilities in terms of measurement resolution, energy consumption, and potential ease of implementation. The solution that best balances these three goals is the RC time constant method. This method will be briefly described and then analyzed according to the following criteria: ease of implementation (cost, overall size, number of external components, etc), measurement resolution, and energy consumption. The analysis will assume there are six capacitive force sensors, each with a capacitance of 20 pF and each must be sampled at a frequency of 10 Hz.

4.2.1 *RC Time Constant Method*

4.2.1.1 Introduction

From basic physics, the time constant, τ, of a first-order system is equal to the time when the system reaches a voltage equal to 63.2% of the final value. For an electrical circuit consisting of a voltage source, resistor, and capacitor, the time constant is equal to the value of $R \cdot C$. The capacitance of the circuit can be calculated by measuring the time constant (discharge time of the capacitor) and knowing the value of R. Fortunately, modern microcontrollers are capable of simultaneously monitoring the voltage across the capacitor and measuring the discharge time. The CC430 microcontroller from Texas Instruments has onboard voltage comparators that can monitor the voltage across the capacitor and determine when the voltage drops below a specified threshold. A schematic showing the potential measurement circuit is shown below in Figure 10.

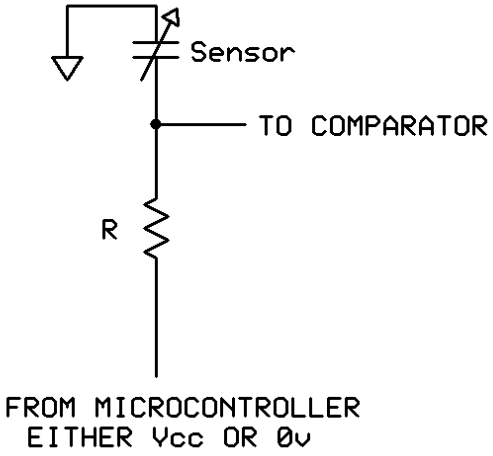

Figure 10 – Schematic for RC time constant measurement circuit

4.2.1.2 Measurement Resolution

The resolution of the capacitance measurement can be calculated by knowing the clock speed of the microcontroller and the discharge time of the capacitive circuit. The voltage comparators on the CC430 microcontroller provide alerts when the voltage across the capacitor drops below 25% of the supply voltage (Vcc). The discharge time will be determined by counting the number of clock cycles of the microcontroller between the start of the discharge and when the capacitor voltage reaches 25% of Vcc. Since the

discharge time will be based on a discharge of 75% of the initial voltage, the discharge time will be longer than the time constant. The calculation below shows the relationship between discharge time and time constant.

$$T_{discharge} = \tau \cdot \ln\left(\frac{Vcc}{0.25 \cdot Vcc}\right) = 1.4 \cdot \tau$$

The CC430 microcontroller has an adjustable clock frequency between 1 MHz and 20 MHz; with higher clock frequencies resulting in higher power consumption. The datasheet for the CC430 shows that 8 MHz is a good balance between power consumption and clock frequency. Unfortunately, the clock frequency on most microcontrollers is susceptible to drifting, caused by changes in supply voltage and temperature. According to the CC430 data sheet, the drift tolerance on the REF0 clock is ± 3.5% over the range of temperature and supply voltage. This issue will be alleviated by adding a precision fixed capacitor and resistor to the circuit board and using the RC time constant of that circuit as a known reference to normalize the sensors readings. To increase the accuracy of the normalization and to increase the resolution of the reference circuit, the value of the precision capacitor will be approximately 10 times larger than the nominal sensor capacitance.

The next circuit parameter to determine is the value of the resistor. To maximize measurement resolution, the value should be as large as possible without bringing extraneous noise into the electrical circuit. The Texas Instruments literature uses a 5.1 MΩ resistor for a capacitive touch screen application circuit (Texas Instruments, 2007). However, this knowledge will only be used as a baseline, since their system is not intended to be a highly accurate measurement device. To balance measurement resolution and noise immunity, a 2 MΩ resistor will be used for the measurement circuit. The corresponding time constant and resolution for this configuration are calculated below. $N_{discharge}$ corresponds to the number of clock cycles of the microcontroller during discharge.

$$\tau = R \cdot C = (2 \cdot 10^{6}) \cdot (20 \cdot 10^{-12}) = 40\mu S$$

$$N_{discharge} = \frac{T_{discharge}}{\left(\frac{1}{f}\right)} = \frac{1.4 \cdot 40 \cdot 10^{-6}}{\left(\frac{1}{8 \cdot 10^{6}}\right)} = 443$$

$$Resolution = \frac{C}{N_{discharge}} = \frac{20 \cdot 10^{-12}}{443} = 0.045\ pF$$

One negative aspect of capacitive sensors is they are susceptible to noise caused by stray capacitance. Stray capacitance can come from many sources: mutual-capacitance between the ground and power planes of the PCB, adjacent components or traces, internal sources within the microcontroller, or external sources such as the human body. The amount of stray capacitance in the sensing circuit from internal sources can be determined by removing the capacitive sensor from the circuit and then measuring the time constant. The stray capacitance can be calculated with the following equation.

$$C_{stray} = \frac{N_{discharge}}{1.4 \cdot R \cdot f}$$

The stray capacitance acts in parallel with the capacitive sensor, which allows the sensor capacitance to be calculated by the following equation.

$$C_{total} = C_{stray} + C_{sensor}$$

Any post-processing of measurement data to determine the sensor capacitance will need to subtract the stray capacitance as shown in the equation above.

4.2.1.3 Energy Consumption

To determine the energy consumption of the capacitance measurement, the measurement process and microcontroller configuration must be understood. The CC430 microcontroller is intended for ultra-low power applications and provides explicit control over many integrated features to decrease power consumption. The highest power consumption is when the CPU is active, called the "active mode", and the full functionality of the CC430 is available. To reduce power consumption, several different "power modes" are provided to control which features are enabled or disabled. The power modes range from low-power mode 0, which, with a 8 MHz clock frequency, has a typical power draw of 270 μW, to low-power mode 4, which has a typical power draw of

3.6 µW. The 8 MHz clock with frequency-locked-loop control (FLL) is available only in active mode and low-power mode 0. FLL control will be required for this application since it is essential to maintaining precise control of the clock frequency. Consequently, the discharge time will be performed in low-power mode 0 to provide the lowest-power consumption possible. Charging the capacitive sensors will be accomplished by applying Vcc to the corresponding capacitive sensor for a minimum amount of time. Since the charge time only needs to exceed a minimum, a low-frequency clock can be used to control the charge time. To minimize the power consumption, low-power mode 3 should be used with a 32768 Hz clock. The flowchart below shows the proposed process and configuration settings for the capacitance measurement.

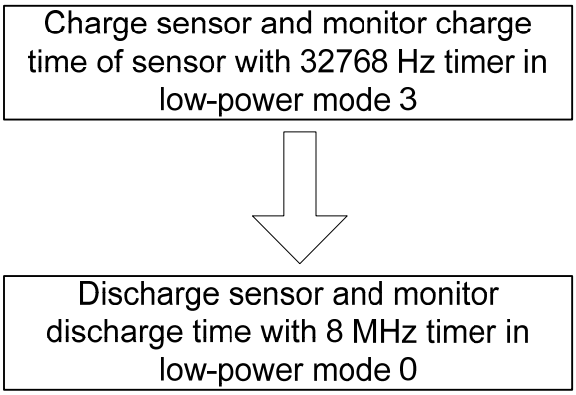

Figure 11 – Flowchart of Capacitance Measurement

As shown in Figure 11, the first process step is to fully charge the capacitive sensors. In terms of energy usage, this step can be decomposed into two parts: first, the amount of stored energy in the capacitive sensors when fully charged and second, the amount of energy used by the CC430 to charge the capacitive sensors. The calculation below shows the amount of energy stored in one capacitive sensor when fully charged.

$$Energy = \left(\frac{1}{2} \cdot C \cdot V^2\right) = \frac{1}{2} \cdot 20 \cdot 10^{-12} \cdot 3^2 = 0.09\, nJ$$

Now the energy can be calculated to fully charge six capacitive sensors and one reference capacitor ten times each.

$$Energy = \left(60 \cdot \frac{1}{2} \cdot C \cdot V^2\right) + \left(10 \cdot \frac{1}{2} \cdot [10 \cdot C] \cdot V^2\right) = \frac{160}{2} \cdot 20 \cdot 10^{-12} \cdot 3^2 = 14\, nJ$$

To calculate the energy required by the CC430 to charge the capacitive sensors, the CC430 supply current, CC430 supply voltage, and charge time must be known. The data sheet for the CC430 lists the max supply current as 3 µA for this configuration at 3 V supply voltage. The corresponding power consumption is calculated below.

$$P_{charge} = I \cdot V = 9\ \mu W$$

The charge time of the capacitor can be calculated with the charge level and the time constant. To ensure adequate sensor accuracy, the capacitor should be within 0.1% of being fully charged before discharging occurs. The charge time can be calculated as shown below.

$$T_{charge} = -\ln\left(1 - \frac{0.999 \cdot Vcc}{Vcc}\right) \cdot \tau = 6.9 \cdot \tau$$

According to the calculation above, the time to charge the capacitor within 0.1% of fully charged is 6.9 time constants. Using the time constant provided in the measurement resolution section results in the following total charge time for a single capacitive sensor.

$$T_{charge} = 6.9 \cdot 40 \cdot 10^{-6} = 0.276\ mS$$

The total energy used to charge the six capacitive sensors and one reference capacitor ten times each is calculated below.

$$U_{charge} = P_{charge} \cdot \left(6 \cdot 10 \cdot T_{charge} + 10 \cdot 10 \cdot T_{charge}\right)$$

$$U_{charge} = 9 \cdot 10^{-6} \cdot 160 \cdot 40 \cdot 10^{-6} = 58\ nJ$$

Now the second process step from Figure 11 can be analyzed in terms of energy usage. To calculate the amount of energy required to measure the discharge time, the CC430 supply current, CC430 supply voltage, and discharge time must be known. The data sheet for the CC430 lists the supply current as 720 µA for this configuration at 3 V supply voltage. The corresponding power consumption is calculated below.

$$P_{discharge} = I \cdot V = 2.2\ mW$$

The discharge time was calculated in the measurement resolution section and is used in the calculations below to determine the energy consumed to measure the sensor capacitance.

$$U_{discharge} = P_{discharge} \cdot \left(6 \cdot 10 \cdot T_{discharge} + 10 \cdot 10 \cdot T_{discharge}\right)$$

$$= 0.0022 \cdot 160 \cdot 1.4 \cdot 40 \cdot 10^{-6} = 20\ \mu J$$

To calculate the total energy consumption to measure the six capacitive sensors and one reference capacitor, the previously calculated energies can be added as shown below.

$$U_{total} = U_{charge} + U_{discharge} = 14\ nJ + 20\mu J = 20.014\ \mu J$$

The average power can be calculated by using the above result and dividing by the total measurement time, in this case one second.

$$P_{average} = \frac{U_{total}}{T_{total}} = 20\ \mu W$$

The calculations shown above demonstrate that the average power consumption for this measurement technique should be sufficiently low to meet the requirements for this system.

4.2.1.4 Ease of Implementation

The previous analyses demonstrated that the RC time constant method can be implemented with one external, passive component per sensor and two external, passive components for the reference circuit. In terms of software code requirements, the method should be reasonably simple to implement with the CC430 microcontroller, especially since the CC430 integrates a sufficient number of voltage comparators to measure all of the sensors.

4.2.1.5 Software Filtering

As discussed in section 4.2.1.2 , capacitive sensors are susceptible to noise from many different sources. One way of reducing the level of noise is to apply a low-pass filter to the sensor measurements. A low-pass filter can be easily implemented in real-time by making consecutive measurements of the sensor and then saving the average value. Unfortunately, implementing this software filtering algorithm would double the energy consumed by measuring the sensors. However, this tradeoff may be necessary to produce acceptable force measurement results. Actual testing will be required before a determination can be made as to whether a low-pass data filter is necessary and if so, whether the increase in energy consumption is detrimental to the performance of the system.

4.3 Design of Capacitive Sensors

4.3.1 *Introduction*

To serve as a capacitive force sensor, the capacitance of the sensor must vary with respect to applied force. As shown earlier, the capacitance of a parallel-plate capacitor can be calculated with the following equation.

$$C = \frac{\epsilon_0 \cdot k \cdot A}{t}$$

The equation above shows that the capacitance of the sensor is linearly related to all of the design parameters. One of the important specifications for a sensor is the sensitivity. It is desirable for the sensor to be sensitive so that small changes in force can be detected. To calculate the sensitivity for each design parameter, the derivative of the equation above was taken with respect to each design parameter.

$$\frac{\partial C}{\partial k} = \frac{\epsilon_0 \cdot A}{t}$$

$$\frac{\partial C}{\partial A} = \frac{\epsilon_0 \cdot k}{t}$$

$$\frac{\partial C}{\partial t} = \frac{-\epsilon_0 \cdot k \cdot A}{2 \cdot t^2}$$

The equations above show two important principals: (1) the sensitivity is positively linear with both the capacitor plate area and dielectric constant and (2) the sensitivity is negative-inversely quadratic with the dielectric thickness. These observations imply that the sensitivity is maximized by minimizing the dielectric thickness and maximizing the dielectric constant and plate area.

Now that the important electrical design parameters are understood, the mechanical analysis can begin to finalize the design. Two design concepts will be presented and analyzed below. Each concept will be analyzed with respect to the ease of implementation and performance.

4.3.2 *Design Constraints and Performance Requirements*

1. The sensors and measurement system must fit within the boundaries of a typical knee replacement assembly.

2. The deflection of the sensors must be small enough to prevent the patient from perceiving a deflection. (Tokuhara, Kadoya, Nakagawa, Kobayashi, & Takaoka, 2004) showed that the mean lateral and medial flexion gaps were 6.7 mm and 1.2 mm when varus and valgus stresses were applied respectively. With this finding, a 0.75 mm (.030") maximum deflection should be adequate to prevent the deflection from becoming noticeable.
3. The sensor must have adequate resolution to determine the force distribution across the knee and to detect a load imbalance. With six sensors and a nominal body weight of 180 lbs, the mean force on each sensor will be approximately 30 lbs. If the goal is to detect a 10% load imbalance within the knee, then the measurement resolution must be less than 1.5 lbs.
4. As discussed in the Section 2.2, the knee is subjected to forces up to 4 times the body weight of the patient. Consequently, the capacitive sensors as a group must be able to safely withstand the same force range as the knee, approximately four times the body weight, or 1000 lbs for a 250 lb person. This implies that each of the six sensors must be able to withstand approximately 167 lbs.

4.3.3 *Sensor Concept # 1 – Allow force to change area of capacitor*

The basic principle for concept # 1 is to utilize the applied force to change the effective area of the capacitor. The dielectric material will act like a bearing between the capacitor plates. Compliant material placed between the capacitor plates will allow capacitor plate # 2 to move with respect to capacitor plate # 1, which changes the area and capacitance of the sensor. A diagram of concept # 1 is shown below.

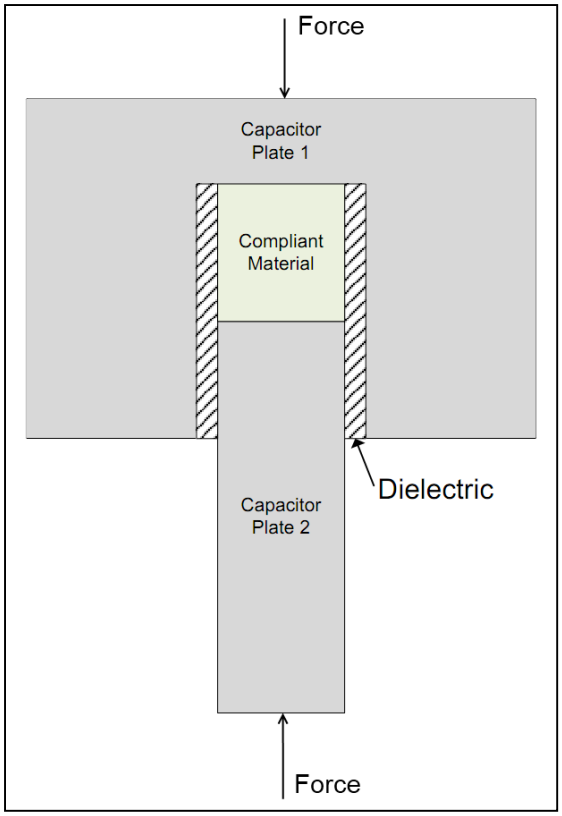

Figure 12 – Diagram of concept # 1 for a capacitive sensor

To fully analyze concept # 1, the capacitance and sensitivity of the sensor must be calculated. A table with all of the pertinent design parameters is shown below.

Description	Variable Name	Nominal Value
Dielectric thickness	t	0.001 in
Outer diameter of capacitor plate # 2	D	0.125 in
Insertion distance of capacitor plate # 2 within capacitor plate # 1 with no load	h	0.125 in
Dielectric Strength of dielectric material	k	2

Table 1 – Design Parameters for Concept # 1

Now that the design parameters have been identified, the capacitance of the sensor with no applied load can be calculated.

$$C = \frac{\epsilon_0 \cdot k \cdot A}{t} = \frac{\epsilon_0 \cdot k \cdot (\pi \cdot D \cdot h)}{t} = 22.1\ pF$$

The sensitivity of the capacitive sensor with respect to the change in height of the compliant material can be calculated by taking the derivative of the equation above with respect to the overlap height, h.

$$\frac{dC}{dh} = \frac{d}{dh}\left(\frac{\epsilon_0 \cdot k \cdot (\pi \cdot D \cdot h)}{t}\right) = \frac{\epsilon_0 \cdot k \cdot (\pi \cdot D)}{t} = 177\frac{pF}{in}$$

The geometry and type of compliant material combine to determine how the capacitive sensor responds to applied force. Both the geometry and material type are undetermined at this point and can be later defined once the required force/deflection response is understood. To simplify this initial analysis, assume that the compliant material is replaced with a spring that has a linear relationship between force and deflection. The equivalent linear spring constant of the compliant material can be calculated by knowing the resolution of the capacitance measurement and the desired force measurement. The following equation calculates the minimum required spring constant for the compliant material.

$$K = \frac{\Delta F \cdot \frac{dC}{dh}}{\Delta C} = \frac{(1.5\ lbs) \cdot \left(177\ \frac{pF}{in}\right)}{0.045\ pF} = 5890\ \frac{lbs}{in}$$

If the compliant material is cylindrically shaped, the spring constant of the cylinder can be calculated with the following equation, where E is the Young's modulus of the material, A is the cross-sectional area of the cylinder, and L is the length of the cylinder.

$$K = \frac{E \cdot A}{L}$$

When considering the space constraints for the orthopedic system, the maximum length of the dielectric material should be approximately 0.25 in. The outer diameter of the compliant material should be smaller than the inner diameter of the dielectric material to allow for expansion of the compliant material due to the Poisson effect. To meet this requirement, an arbitrary diameter of 0.115 in was chosen. Using these two pieces of information allows the young's modulus of the compliant material to be calculated, as shown below.

$$E = \frac{L \cdot K}{A} = 142\ Ksi$$

By comparing the calculated young's modulus with a table of typical engineering materials, the closest material is polypropylene, with a young's modulus of 220 Ksi. Polypropylene is not a desirable material choice for several reasons: the stress-strain relationship is typically non-linear, the stress-strain relationship is highly dependent on temperature, and the material is prone to creep. For these reasons, a metallic material with a non-conductive coating is desirable, but unfortunately, the metallic engineering material with the lowest young's modulus is aluminum at 10,000 Ksi. To compensate for the increased young's modulus of aluminum, the cross-sectional area of the compliant material would need to be decreased by a factor of 70. However, the resulting peak compressive stress within the compliant material would exceed the yield stress, even for aircraft grade aluminum. Consequently, no material meets the necessary design constraints and the next sensor concept will be examined for a potential solution.

Another potential issue with this sensor concept is that each capacitor plate would have to be connected to the printed-circuit board (PCB). For six sensors, this corresponds to twelve connections to the PCB. As stated earlier, capacitive sensors are susceptible to stray capacitance and external wires between the capacitor plates and PCB would substantially increase the stray capacitance. It is possible however, for capacitor plate # 1 to be common among all of the sensors and to attach the other capacitor plates directly to PCB. However, the difficulty here would be to ensure that the solder joints on the PCB are not subjected to any mechanical stress which would occur if there were lateral loads on any capacitor plate # 2. Lateral loads could potentially cause fatigue cracks in solder joints on the PCB and could result in intermittent connection failures.

4.3.4 *Sensor Concept # 2 – Allow force to change dielectric thickness*

The basic principle for concept # 2 is to utilize the applied force to change the dielectric thickness of the capacitor. A diagram of concept # 2 is shown below.

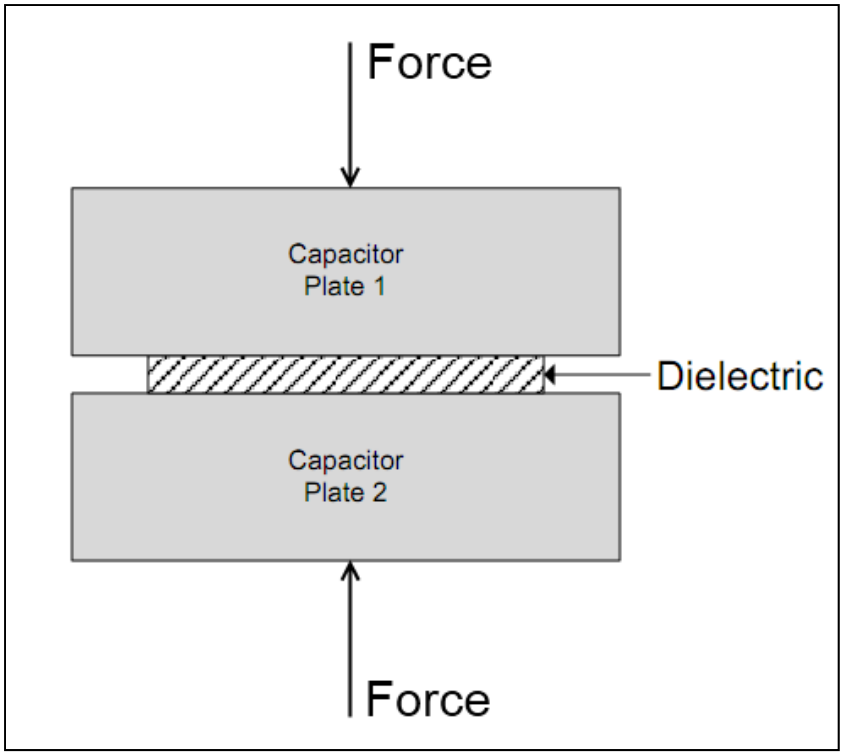

Figure 13 – Diagram of concept # 2 for a capacitive sensor

To fully analyze concept # 2, the capacitance and sensitivity of the sensor must be calculated. A table with all of the pertinent design parameters is shown below.

Description	Variable Name	Nominal Value
Dielectric thickness	t	0.015 in
Length of capacitor plates	L	0.25 in
Width of capacitor plates	W	0.25 in
Dielectric strength of dielectric material	k	2

Table 2 – Design Parameters for Concept # 2

Now that the design parameters have been identified, the capacitance of the sensor with no applied load can be calculated.

$$C = \frac{\epsilon_0 \cdot k \cdot A}{t} = \frac{\epsilon_0 \cdot k \cdot (L \cdot W)}{t} = 1.87\ pF$$

The sensitivity of the capacitive sensor with respect to change in thickness of the dielectric material can be calculated by taking the derivative of the above equation with respect to the dielectric thickness, t. The equation below shows that the sensitivity is

nonlinear with respect to dielectric thickness. A graph showing the relationship between sensitivity and dielectric thickness is also shown below.

$$\frac{dC}{dt} = \frac{d}{dt}\left(\frac{\epsilon_0 \cdot k \cdot (L \cdot W)}{t}\right) = -\frac{\epsilon_0 \cdot k \cdot (L \cdot W)}{t^2} = 125\frac{pF}{in}$$

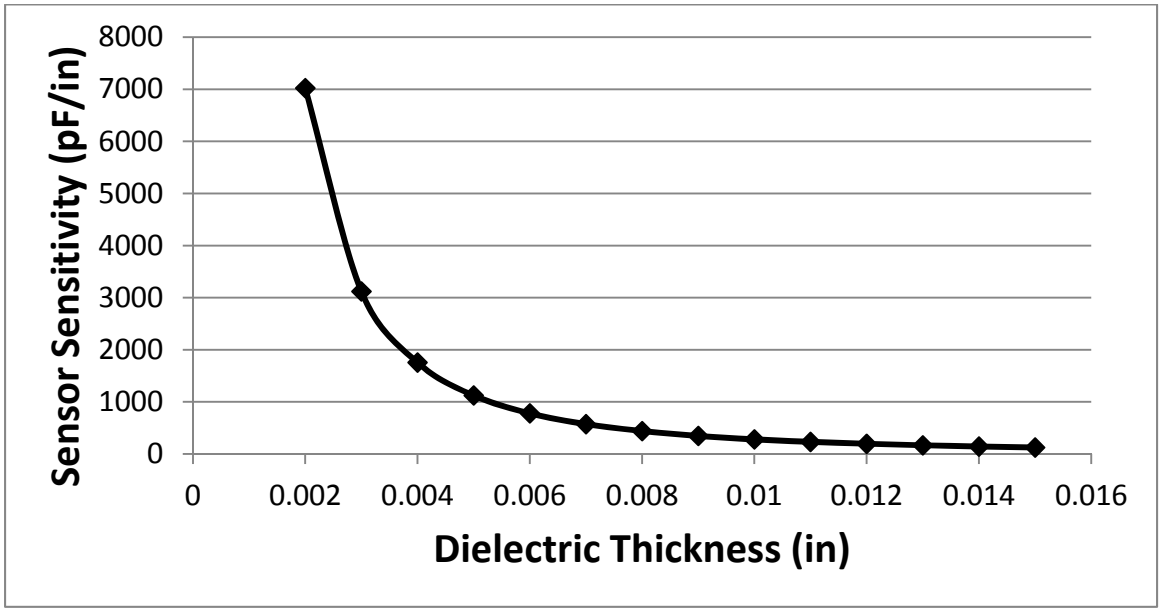

Figure 14 – Graph showing non-linear relationship between dielectric thickness and sensor sensitivity

The geometry and type of compliant material combine to determine how the capacitive sensor responds to applied force. Both the geometry and material type are undetermined at this point and can be later defined once the required force/deflection response is understood. To simplify this initial analysis, assume that the compliant material is replaced with a spring that has a linear relationship between force and deflection. This assumption may not be entirely valid, but the result will be only be used to obtain an approximate order of magnitude of the specifications for the dielectric material. Once this result has been calculated, a more thorough analysis will be performed. The equivalent linear spring constant of the compliant material can be calculated by knowing the resolution of the capacitance measurement and the desired force measurement. The following equation calculates the minimum required spring constant for the compliant material.

$$K = \frac{\Delta F \cdot \frac{dC}{dh}}{\Delta C} = \frac{(1.5\ lbs) \cdot \left(125\ \frac{pF}{in}\right)}{0.045\ pF} = 4160\ \frac{lbs}{in}$$

If the compliant material is shaped like a rectangular plate, the spring constant of the cylinder can be calculated with the following equation, where E is the Young's modulus of the material, A is the cross-sectional area of the plate, and t is the thickness of the plate.

$$K = \frac{E \cdot A}{t}$$

Rearranging this equation and solving for young's modulus allows this parameter to be calculated, as shown below.

$$E = \frac{t \cdot K}{A} = 1.0\ Ksi$$

The calculated young's modulus above is extremely low and is on the order of rubber materials. However, due to the length to thickness aspect ratio of the dielectric material, the high bulk modulus of rubber, the high Poisson's ratio of rubber, and the boundary conditions, the preceding analysis is invalid. If the top and bottom surfaces of the rubber are not completely free to move laterally, the stiffness of the dielectric material will be many times larger than was calculated above (McCrum, Buckley, & Bucknall, 1997). Lubricant may help reduce the stiffness of the dielectric by allowing lateral movement, but this may not be reliable over the life of the implant. Thus, rubber dielectric material does not appear to meet the necessary performance requirements for the design that was considered.

Instead of using compliant material shaped like a rectangular plate, a torus was chosen for the geometry to decrease the effective "stiffness" of the material. Also, the torus was slightly inset into one of the capacitor plates to prevent overstressing the torus. The disadvantage of this geometry is that the allowable force range is decreased. Theoretical calculations of the relationship between force and deflection of a rubber torus were not performed due to the high mechanical strains and a lack of trusted material properties.

One advantage of this sensor concept over concept # 1 is that one half of the capacitor plates could be embedded within the PCB and the other half of the capacitor plates could be a common piece of metal. This configuration would result in only one external connection between the common ground plate and the PCB. Also, the PCB would not be subjected to moment-type loads which could induce fatigue cracks in solder joints. For these reasons, sensor concept # 2 seems to have fewer inherent issues with connectivity, manufacturability, and reliability.

4.4 Arrangement of Sensors

The layout of the sensors is important because it will determine how the forces are distributed among the sensors and how the resultant loads will be calculated. Anterior-posterior and lateral-medial symmetry were used to simplify the data analysis. As discussed previously, the proposed load sensing system will have six sensors as shown below in Figure 15, which is slightly different than previous researchers.

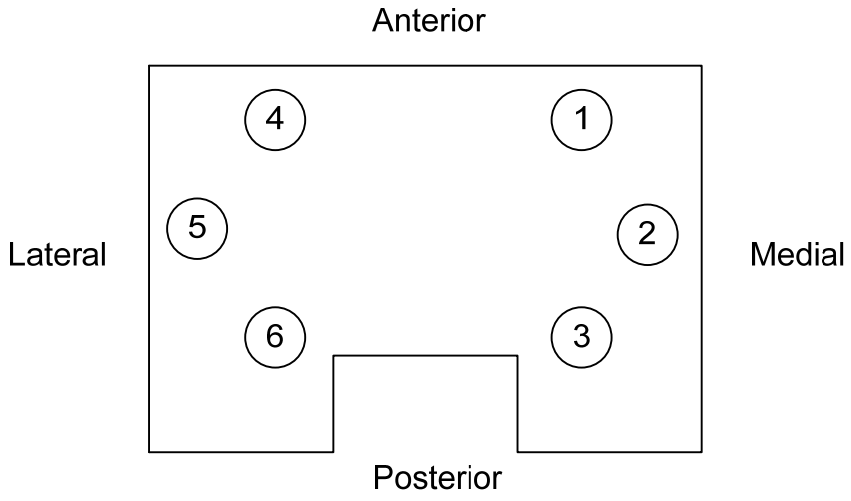

Figure 15 –Arrangement of Force Sensors in Tibial Component

A pioneering system that experimentally measured forces in the knee was (Kaufman, Kovacevic, Irby, & Colwell, 1996). This system used four sensors symmetrically placed in the anterior-posterior and lateral-medial directions. For the system proposed in this paper, six sensors was chosen because it should provide a better estimate of the load distribution in the anterior/posterior direction, since four sensors can only linearly

interpolate between the anterior and posterior sensors. However, six sensors create a statically indeterminate system, which increases the complexity of the load distribution calculations. Additionally, the geometry of the tibial component and polyethylene bearing surface may be complex, which makes a theoretical analysis of the system deflection very difficult. Although the report from (Bergmann, Graichen, Rohlmann, Westerhoff, B. Heinlein, & Ehrig, 2008) was specifically concerned with strain gages, their conclusions generally show that the geometry surrounding the sensors is very important in determining what loads act on the sensors. These findings imply that a combination of experimental data and finite element analysis software (FEA) should be used to understand the general relationship between the sensor measurements and applied loads.

Chapter 5 – Wireless Data Transmission

5.1 Introduction

Wireless communication has become ubiquitous in devices today and consequently, the technology has matured to the point where off-the-shelf systems can be used with great results. As such, an RF circuit developed for the CC430 microcontroller will be used for this application (Texas Instruments, 2010). Two systems will be needed for data transmission; one that is embedded within the implant and another that serves as a base station to receive data from the implanted system. The primary focus of this chapter will be on the implanted system because the base station does not have many of the design constraints of the implanted system. The implanted system will use simplex communication due to energy constraints from enabling duplex communication. Consequently, the embedded system will only transmit data and the base station will only receive data. Future versions of the system could implement duplex communication between the embedded system and the base station, but this feature is not necessary to create a working force measurement system.

5.2 Hardware and Electrical Design

RF data transmission has been successfully used on all of the previous instrumented knee implant systems. However, these systems could use a higher power transmitter than the proposed system because the previous systems did not have the power supply limitations of the proposed system. Some consequences of this energy limitation are the power of the transmitter, the data transmission rate, and the transmission range. The transmitter power is directly affected by the limitations of the power supply, as shown on the data sheet for the CC430. As a consequence of reduced transmitter power, the data transmission rate must be decreased to account for the reduced signal-to-noise ratio.

Another potential issue with RF data transmission is the effect of the human body on the signal-to-noise ratio. (Bashirullah, 2010) showed that frequencies near 900 MHz were optimal, due to reduced absorption of radio waves with biological tissue. Fortunately, the application circuit developed by Texas Instruments can be configured to 915 MHz, whcih

should provide near optimal transmission of data through the biological tissue and should help to maximize the signal-to-noise ratio.

5.3 Software Configuration

The primary constraint for RF transmission is the energy consumption for transmitting a full set of data. According to the data sheet for the CC430, the supply current at 0 dBm output power is 18mA for TX transmission. The CC430 has a built-in voltage regulator for the RF electronics. Assuming a constant supply voltage to the RF electronics, the corresponding power consumption is 54 mW. This consumption level is significantly more than for normal operation of the CC430 microcontroller; therefore, the data transmission time should be minimized to reduce the overall energy consumption. Several configuration settings will be discussed below to potentially reduce the transmission time and correspondingly, the energy consumption.

With six sensors and one reference capacitor, 70 data points will be collected per second at a 10 Hz sampling rate. Each data point will be a number approximately between 150 and 5500. Since numbers over 255 require 16 bits to realize the number in a binary representation, these data points would normally be stored as 16 bits. However, the stored data can be halved by subtracting each sensor reading from a specified number such that all of the data is now in an 8 bit representation. Therefore, each second of measurement time will collect 560 bits of data and ten seconds will yield 5.6 kilobits of data. The transmission rate of the CC430 is configurable between 0.6 and 500 kBaud. However, not all RF systems can effectively use high data rates due to potential issues with RF noise. Testing with the proposed system showed that data rates above 60 kbps caused issues with noise and failed CRC checks. For GFSK modulation, the data rate is equivalent to the baud rate, so the data transmission rate can be configured between 0.6 and 60 kilobits per second (kbps). The dataset must be divided into packets which typically include the following: 2 byte preamble, 2 byte sync word, variable length set of data, and one byte cyclic redundancy check (CRC). If the transmission rate is set to the maximum and the packets are 64 bytes long, than the total transmission time would be 102 milliseconds. Using the power consumption calculated above, which is a

conservative load estimate because it does not account for the power consumption decreasing with the supply voltage, the total energy consumed during this time would be 5.5 millijoules. With this energy consumption, a storage capacitor of 2 mF would drop from 3.5 V to 2.6 V, which implies the device should have adequate stored energy to transmit ten seconds of collected data.

Chapter 6 – Experimental Setup

6.1 Introduction

Before testing on the previously described system could be completed, the tibial tray had to be designed and manufactured, the capacitive force sensors had to be manufactured, and a gait simulator had to be developed.

6.2 Design of Tibial Component

As discussed in Section 2.3, a knee implant essentially has two distinct components: the component that attaches to the tibia and the component that attaches to the femur. The system proposed in this paper requires that the tibial component be completely redesigned. When designing the new tibial component, there were many physical, structural, and electrical requirements as identified below:

- The dimensional boundaries of a typical implant could not be exceeded
- Forces acting on the knee had to be transmitted through the piezoelectric transducer to maximize the performance of the PEHS
- The mechanical design must accommodate the electrical circuit board
- The mechanical design must not create a Faraday's Cage that could obstruct RF transmission
- The capacitive force sensors must be shielded from biological tissue to prevent stray capacitance effects
- The capacitive force sensors must be located such that the distribution of forces along the tibial component could be determined.

Modifications to the polyethylene bearing surface were intended to be minimal to maintain compatibility with existing femoral components. The bearing surface on the polyethylene part was designed as a planar surface to allow the gait simulator to apply loads to the tibial component; for actual in-vivo testing, the bearing surface would have a traditional design to provide lateral stability to the femoral component. Pictures of the final assembly are shown below in Figure 16, Figure 17, and Appendix B.

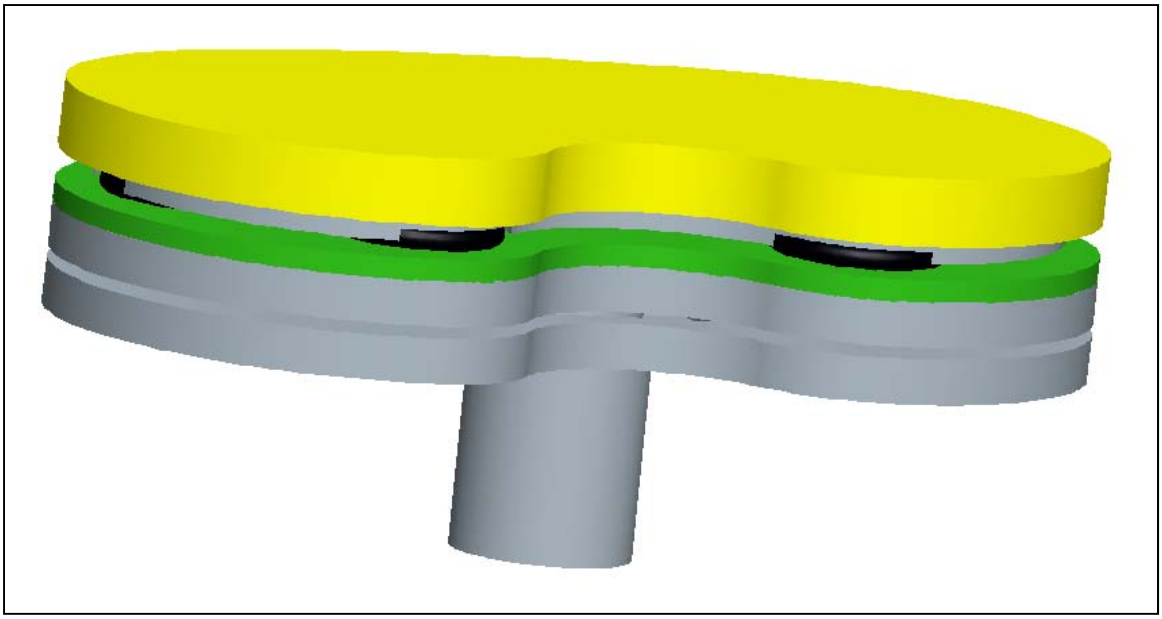

Figure 16 – Picture of final knee implant from Pro-Engineer

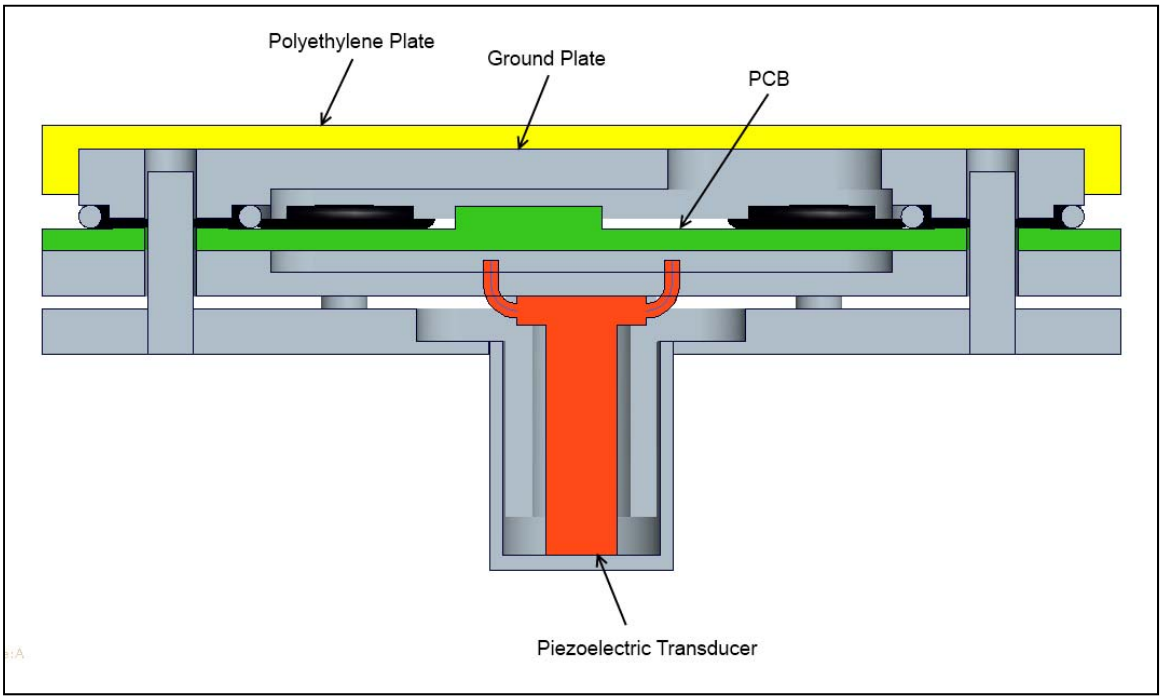

Figure 17 – Cross-section of final knee implant showing layout of various components

Throughout the development of the tibial component, prototypes were manufactured for testing purposes. Since these prototypes were not intended for in-vivo testing,

biocompatible materials were not required. As such, aluminum and polyoxymethylene (acetal) were common materials since they have good machinability and availability.

6.3 Capacitive Force Sensors

Multiple designs for the capacitive forces sensors were proposed in Section 4.3, and unfortunately, no design was found that met the performance requirements. Sensor concept # 1 did not meet all of the performance requirements and was difficult to manufacture because of the thin dielectric material and multiple sensor connections, whereas sensor concept # 2 was easier to manufacture, but had even worse performance characteristics than sensor concept # 1. Despite this finding, the sensors can be designed so that some of the requirements are met. The final design is shown below in Figure 18. Nitrile rubber was chosen as the compliant material because nitrile has excellent mechanical resiliency when compared to other rubber materials.

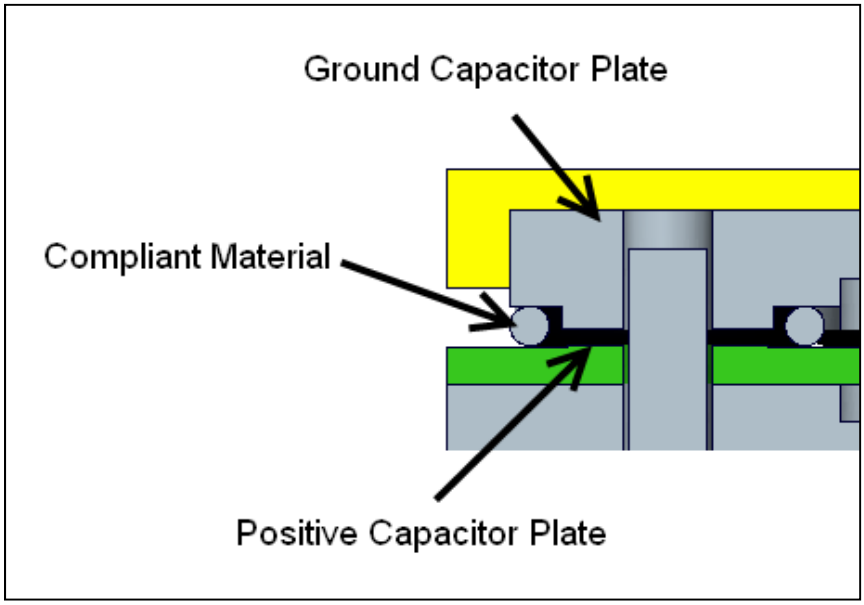

Figure 18 – Final design of capacitive force sensor

6.4 Gait Simulator

A gait simulator, designed and constructed by Lee Alexander (a colleague) at the University of Minnesota, was used for application testing of the device. The simulator

used four pneumatic actuators to apply loads to the device under test (DUT). The supply hose for each actuator contained an on/off valve, pressure regulator, and a variable supply orifice. The on/off valves were triggered with a microcontroller to have a 0.5 second ON time and 0.5 second OFF time. The variable supply orifice was used to limit the rate at which pressure could increase in the actuator cylinder. If the supply orifice were set to a wide-open position, the pressure in the actuator would mimic a square wave function with the on/off valve controlling the dwell times at high and low pressure. If the supply orifice were set to a nearly-closed position, the pressure in the actuator would mimic a saw tooth function with the pressure rising slowly from low to high than dropping off sharply when the on/off valve closed, see Figure 20. With the supply orifice and pressure regulator unique to each actuator, the air pressure in each actuator could be precisely controlled which provided the ability to test unequal loading on the DUT. A picture of the gait simulator is shown in Figure 19 below.

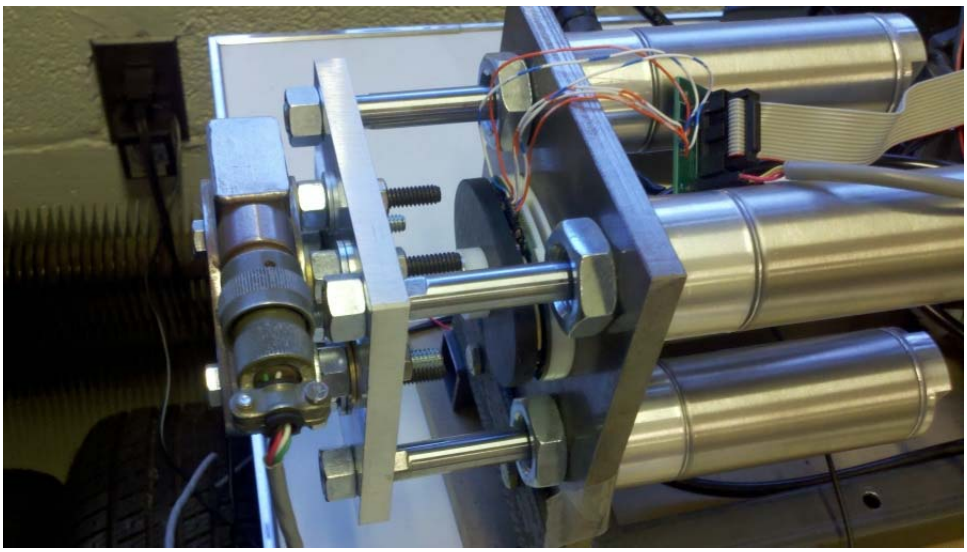

Figure 19 – Picture of Gait Simulator

The total peak load applied to the DUT can be calculated by knowing the air pressure and effective diameter of the actuators. The following calculations and table show the total peak applied load assuming the air pressure is equal among the actuators.

$$F_{Total} = 4 \cdot P \cdot \left(\frac{\pi D^2}{4}\right)$$

Air Pressure (psi)	Calculated Peak Force (lbs)	% of Body Weight for 170 lb person
10	71	42%
15	106	62%
20	141	83%
25	177	104%
30	212	125%
35	247	146%
40	283	166%
45	318	187%
50	353	208%
55	389	229%
60	424	249%

Table 3 – Calculated loads for gait simulator

To examine the load profile applied by the actuators and to validate the calculated loads from Table 3, a load cell was placed on the gait simulator to measure the total resultant force. Figure 20 shows the load profile that was measured when the actuators had 40 psi of pressure. The typical peak force measured during the loading cycle in Figure 20 was 276 lbs, which closely matches the calculated load of 283 lbs.

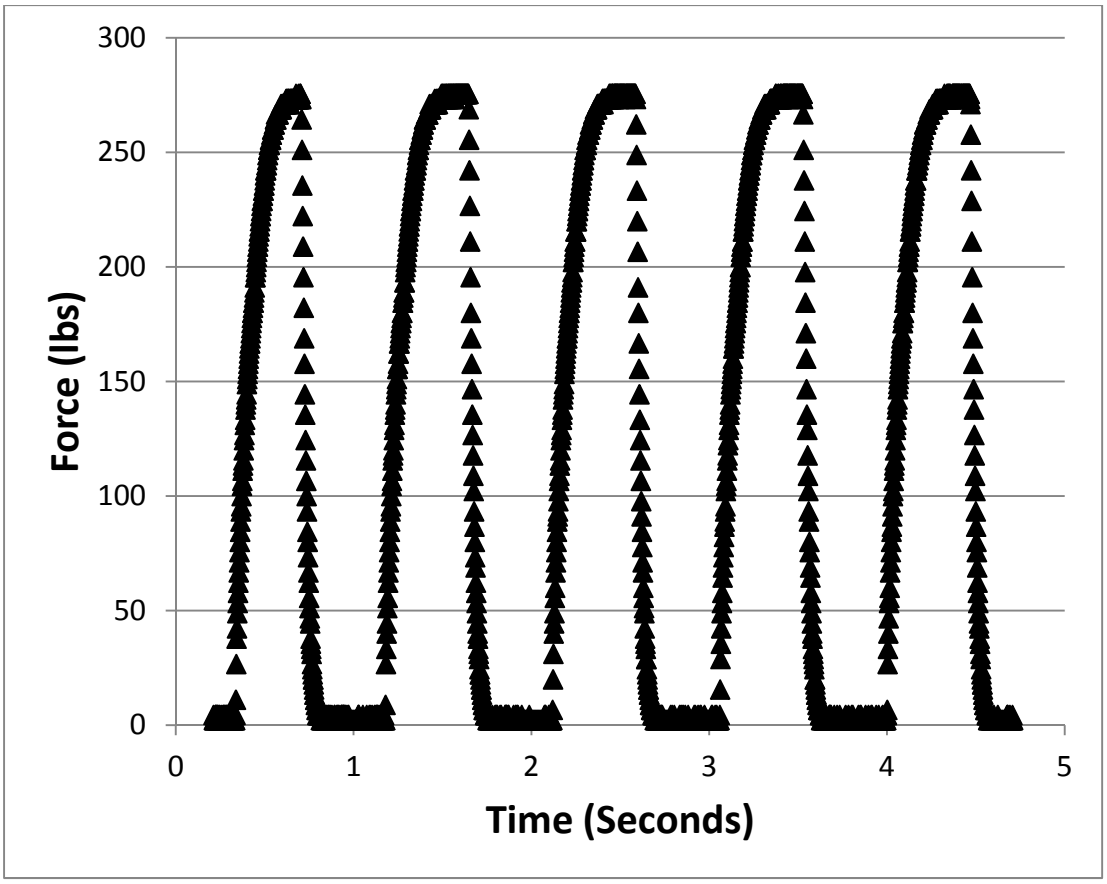

Figure 20 – Typical loading cycle with gait simulator at 40 psi air pressure

Chapter 7 – Results

7.1 Introduction

A series of tests were performed to understand the performance of the instrumented tibial tray. The results will be presented according to these primary topics: piezoelectric energy harvesting, capacitive force sensing, and system power consumption.

7.2 Piezoelectric Energy Harvesting

Testing was performed on the PEHS to determine the relationship between applied force and harvested energy. As discussed previously, the storage capacitor had a capacitance of 2mF and a peak voltage of 3.5 volts. The stored energy in the capacitor can be calculated by the following equation.

– – J

For all testing, the instrumented implant was placed on the gait simulator and the storage capacitor voltage was monitored with an Agilent TDS2022 oscilloscope. The four pressure regulators were all set to the same pressure to ensure even loading on the piezoelectric transducer. A plot showing a typical charging cycle is shown below in Figure 21.

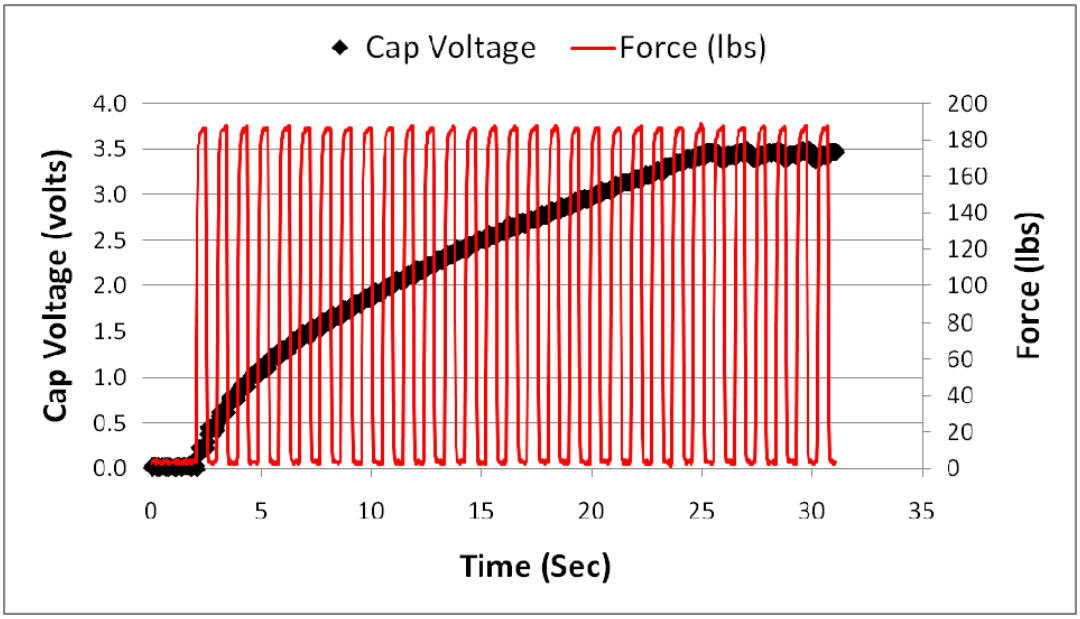

Figure 21 – Typical charging cycle for 188 lbs nominal peak force

The table below shows the full set of test results for various input forces applied to the piezoelectric transducer.

Nominal peak force (lbs)	Number of steps for storage capacitor to reach 3.5 volts	Average energy harvested per step (μJ)
59	Did not charge	N/A
89	121	95.5
122	55	210
154	33	350
188	23	503
217	19	608
256	15	771
284	13	889
316	11	1051
385	10	1156
382	9	1284

Table 4 – Performance of piezoelectric energy harvesting power supply

The primary observation from this table is the number of steps required to fully charge the storage capacitor, which ranges from infinity to 9 steps, depending on the input force. This result is very important because it determines how long the patient must be active before the system can begin to measure forces within the knee.

To calculate the average power of the PEHS, the average energy harvested per step can be divided by the number of steps per second, which in this case is one. Figure 22 below shows a graph of the PEHS performance with respect to applied force.

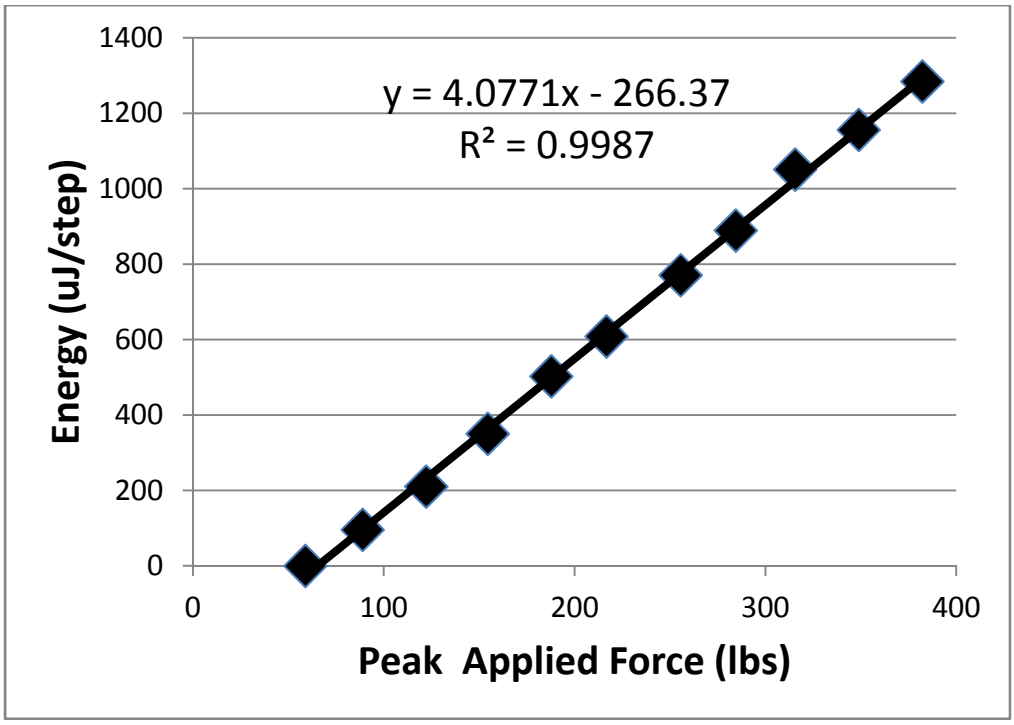

Figure 22 – Relationship between harvested energy of PEHS and applied force

The graph illustrates two important observations that may not have been apparent from the table. The first important observation is that the performance of the PEHS is linear for the range of forces that were tested. As described in Section 3.2, the expectation was that the harvested energy per step would increase as a function of the applied force squared. This discrepancy is a result of the LTC3588 implementing a fixed threshold switching circuit, since the capacitor on the input side of the LTC3588 can only charge to the upper threshold voltage, which is independent of applied force. When the voltage on the input capacitor reaches the upper threshold voltage, the LTC3588 transfers charge from the input capacitor to the storage capacitor until the voltage on the input capacitor reaches the lower threshold voltage. The charge/discharge cycle of the input capacitor will continue until the load on the piezo becomes constant. Consequently, the quantity of charge/discharge cycles of the input capacitor will be approximately proportional to the applied force. Since each discharge cycle of the input capacitor delivers a fixed amount of charge to the storage capacitor, the energy delivered to the storage capacitor will be proportional the applied force. The graphs below further explain the process that was previously described.

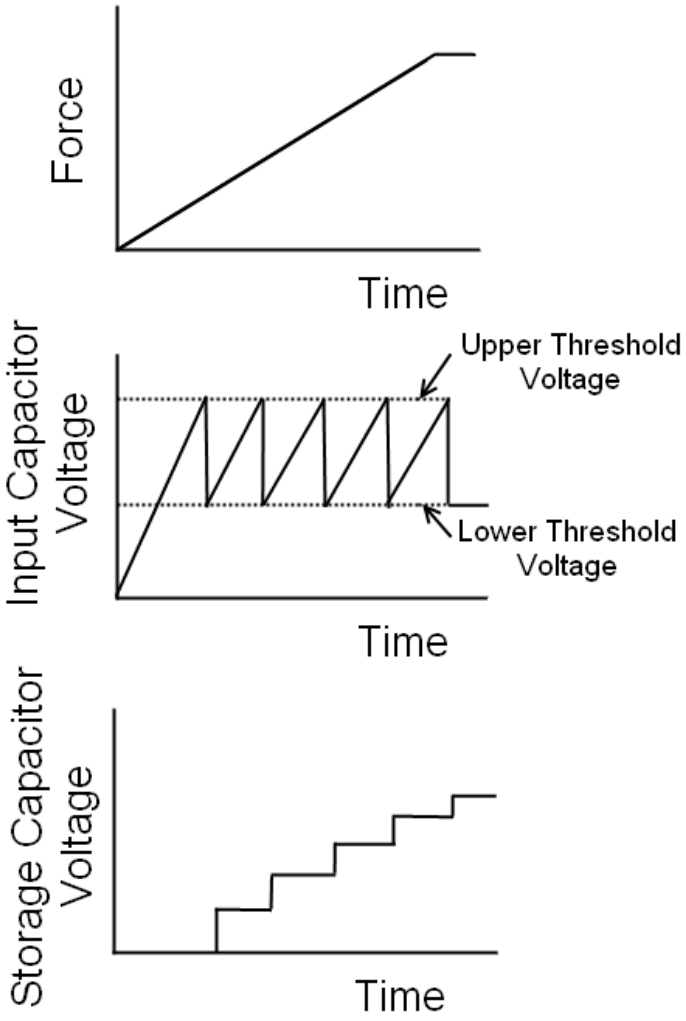

Figure 23 – The top graph shows the force linearly increasing on the piezo transducer. The middle graph shows the voltage on the input capacitor which is coupled to the piezo transducer by a full-wave rectifier. The bottom graph shows the voltage on the storage capacitor.

If the LTC3588 were to implement a max-voltage switching circuit, the performance of the PEHS would follow the expected trend and the performance would be significantly better than was found here.

The second important observation is that a minimum force of 70 lbs is required to start harvesting energy with the PEHS. This requirement is due to the piezoelectric transducer

not outputting a high enough voltage to exceed the minimum threshold on the LTC3588 device.

7.3 Capacitive Force Sensing

As discussed in Section 4.2.1.5, a method was developed to apply a low-pass filter to the data in real-time. Without this filter, the sensor readings showed some minor noise. The final measurement process is outlined in state-diagram form in Figure 23.

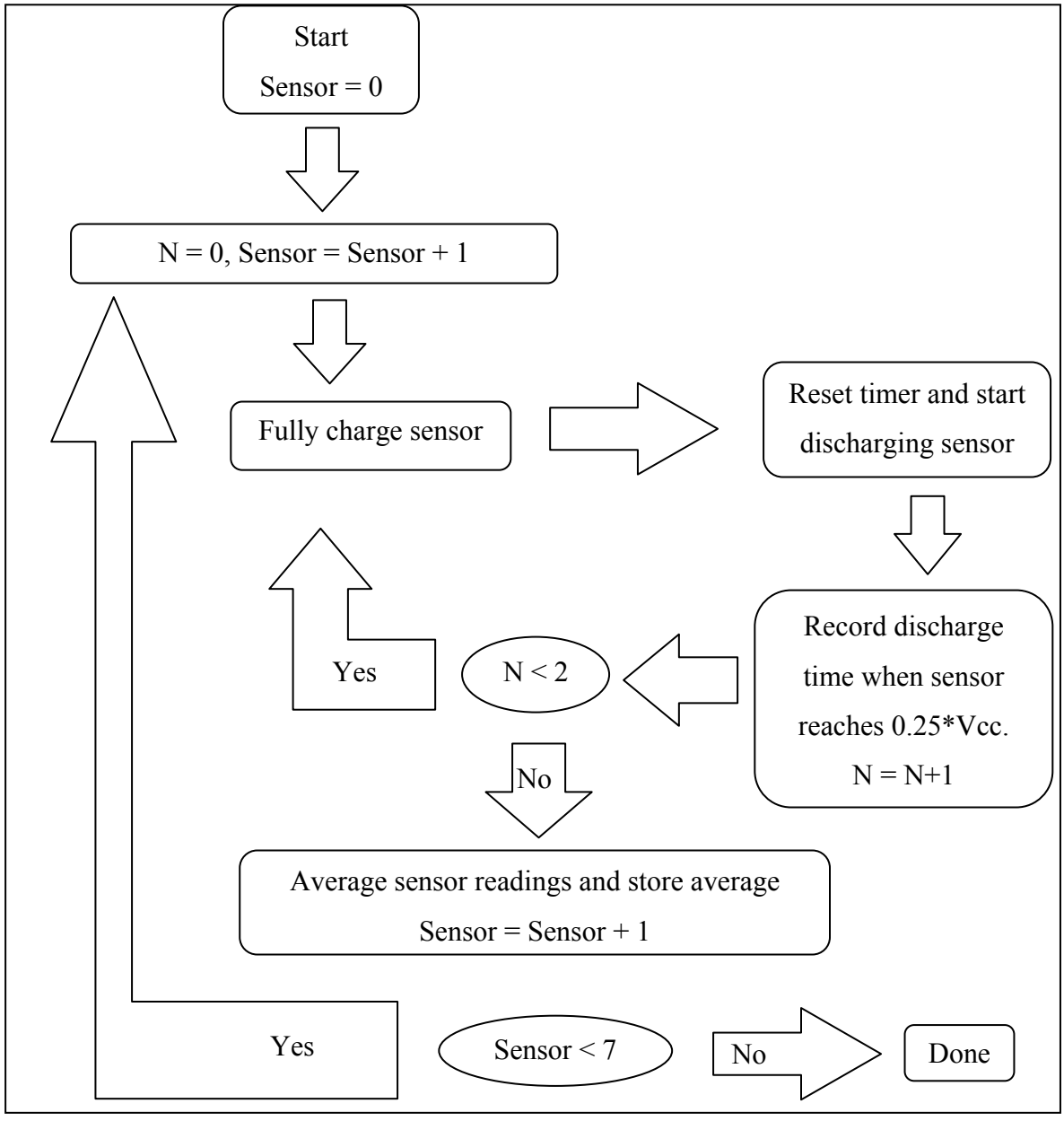

Figure 24 – State Diagram for Capacitive Sensor Measurements

7.3.1 *Relationship between Discharge Time and Capacitance*

To verify the measurement theory presented in Section 4.2.1, tests were performed with a variety of precision capacitors to relate the discharge time and capacitance. The data from this testing is shown below in Figure 24.

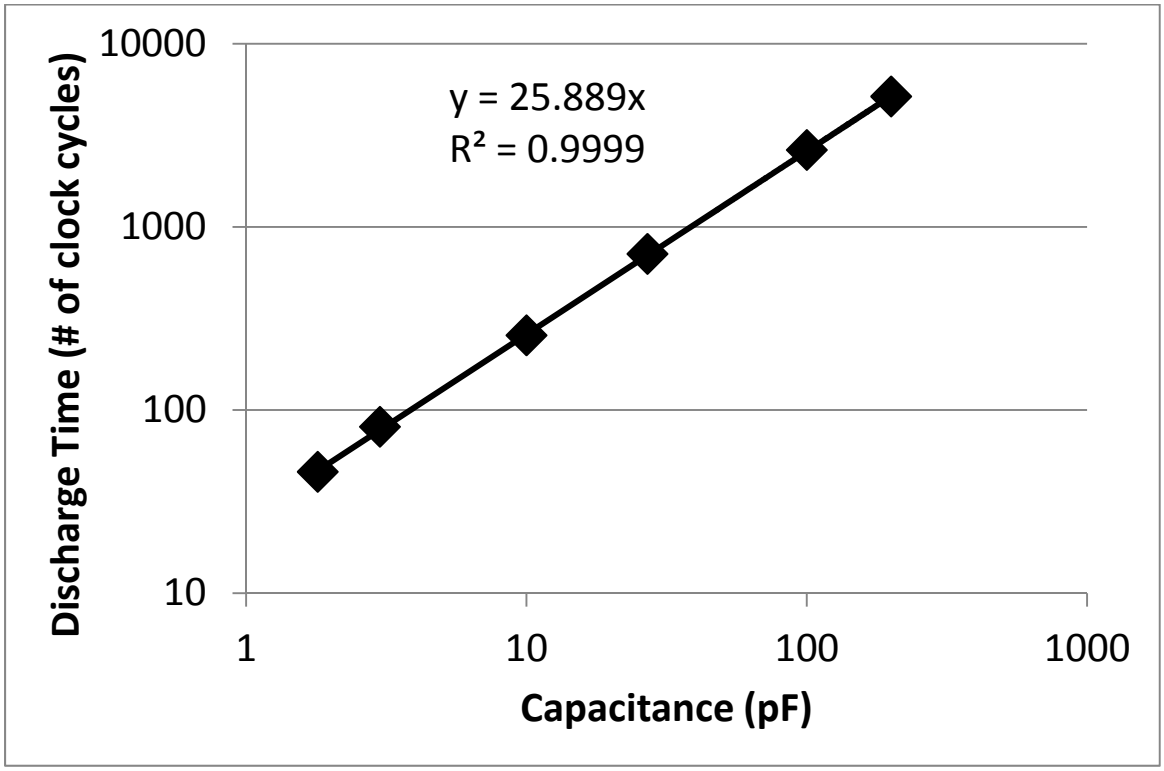

Figure 25 – Relationship between discharge time and capacitance

The test results showed a very good linear correlation between capacitance and discharge time, as was predicted by theory in section 4.2.1.1.

Another test was performed to monitor the voltage of the capacitive sensor during the measurement process. To do this, an oscilloscope probe was connected to one of the capacitive sensors. Unfortunately, the data sheet for the oscilloscope probe showed that the probe will impart a 10 to 15 pF capacitive load onto the sensor. Consequently, the data from this test cannot be used to accurately measure the sensor capacitance and

should only be used to demonstrate the approximate shape of the charge/discharge curve. The data from this test is shown below in Figure 25.

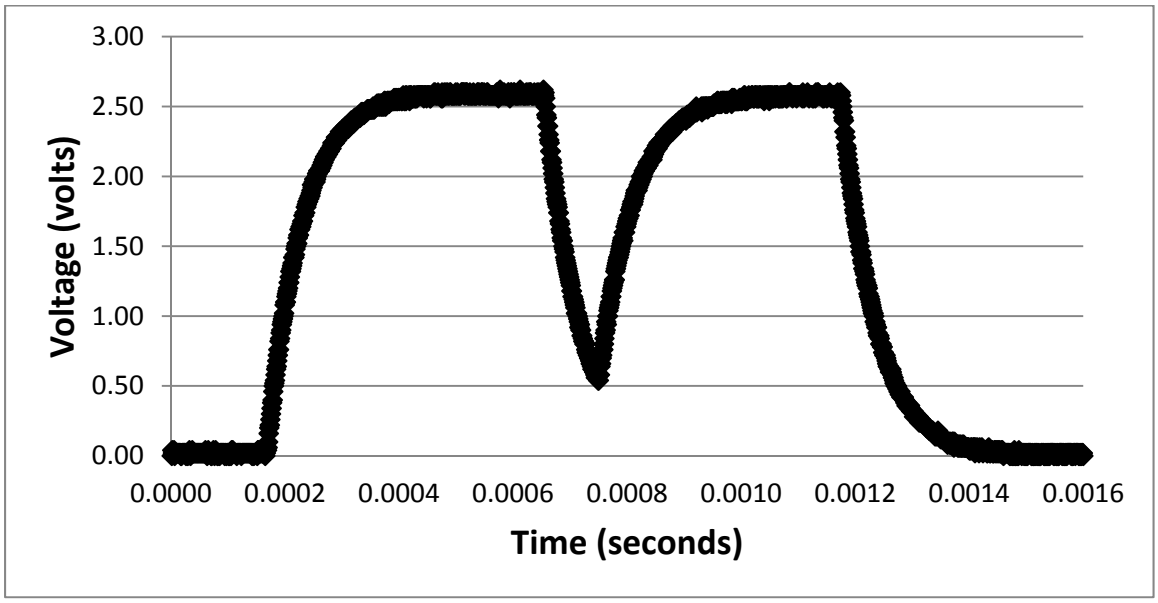

Figure 26 – Charge / discharge cycle for capacitance measurement

One observation from the graph above is the charge time, which is approximately 7 times greater than the time constant. This result demonstrates that the charge time is adequate to ensure the sensor is fully charged before the measurement is taken.

7.3.2 *Relationship between Capacitance and Force*

Before the capacitance of the sensors can be determined, the stray capacitance for each measurement circuit must be calculated. As discussed in Section 4.2.1.2, the stray capacitance can be calculated by disconnecting the capacitive sensors from the measurement circuit and then measuring the time constant of each circuit. Table 5 below shows the calculated stray capacitance for each measurement circuit. The stray capacitance on sensor # 3 was significantly higher than the other sensors. Unfortunately, the root cause for this result was never fully understood

Sensor #	Calculated Stray Capacitance (pF)
1	7.49
2	8.21
3	14.2

4	8.97
5	6.63
6	8.61

Table 5 – Calculated Stray Capacitance for Each Measurement Circuit

The capacitive sensors were calibrated by placing the device on the gait simulator and correlating the load cell force with the corresponding senor measurements. The test was performed as follows.

1. Place the implant in the gait simulator
2. Set the air pressure to the minimum level
3. Turn the simulator ON and obtain measurement data for several cycles
4. Increase the air pressure by 5 psi
5. Repeat steps 3 and 4 until the maximum air pressure has been reached
6. Repeat steps 2 through 5

Figure 26 below shows the starting orientation of the implant in the gait simulator.

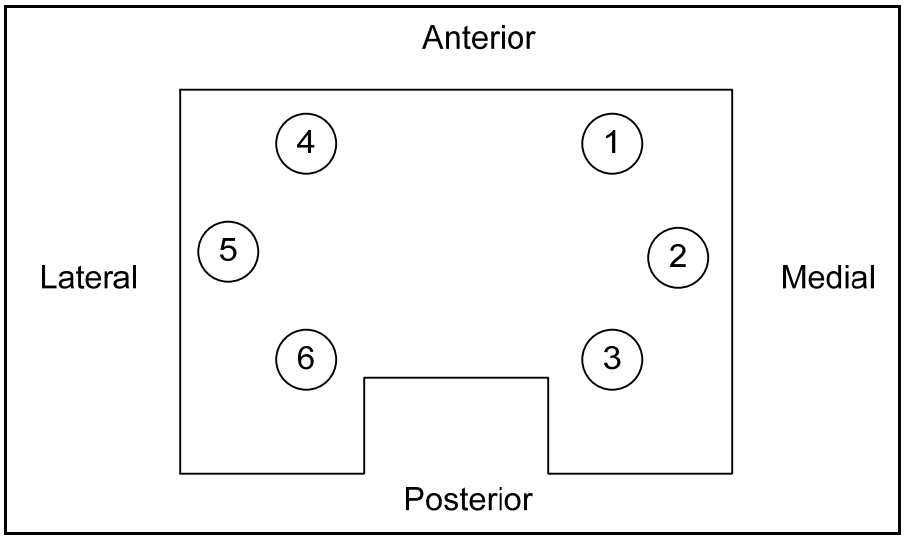

Figure 27 – Layout of capacitive sensors in gait simulator

The capacitive sensor measurement data from this sensor orientation is shown below in Figure 27. Some interesting observations are apparent from this graph: the relationship between force and capacitance is different between sensors, the capacitance of each sensor is linear with applied force, and each sensor shows some variation in capacitance

for a single level of applied force. The first observation does not necessarily indicate a problem, because the load on each sensor may not be equal due to the location of the applied force and the deflection of the polyethylene component and ground plate. Even if the previous hypothesis is false, the difference in sensors can be accounted for by calibrating each sensor. The third observation indicates that the sensors potentially have issues with repeatability, possibly due to unstable mechanical properties of the rubber dielectric material.

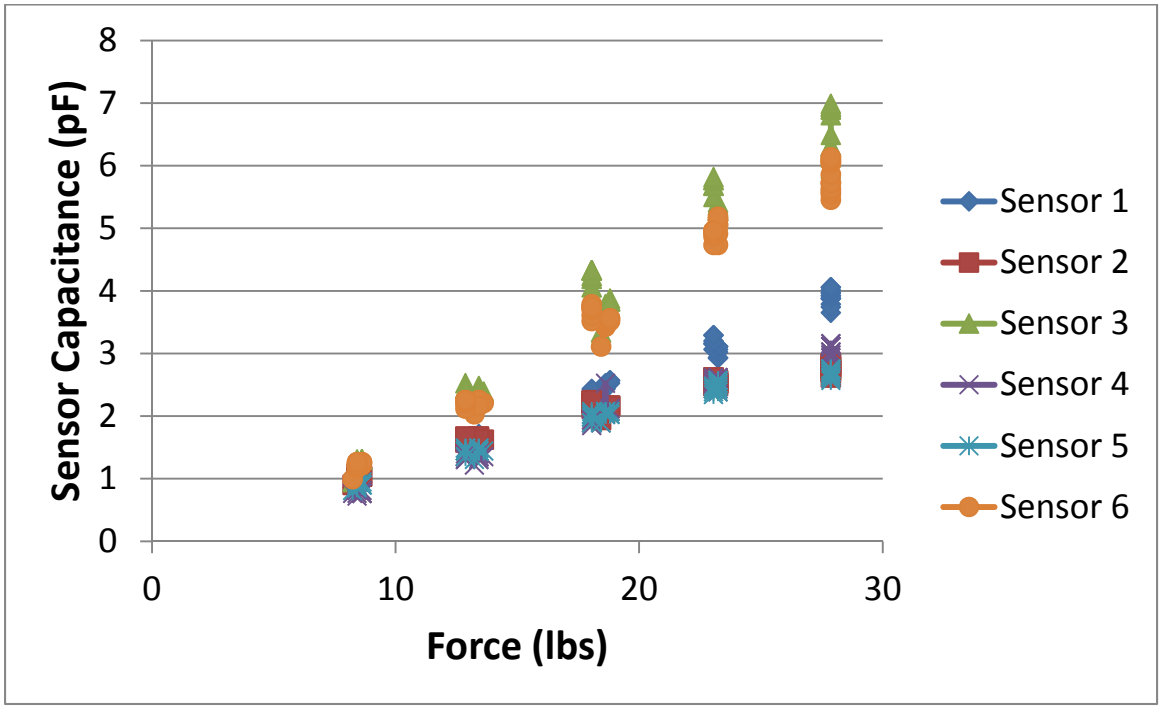

Figure 28 – Relationship between measured sensor capacitance and force. Important note: The load cell measured the total force applied to all of the sensors. This force was divided by six to obtain the force applied to each individual sensor.

Since the force applied to each individual sensor was not measured during testing, it is very difficult to ascertain if the load were equal among all of the sensors or not. To determine if the results from the previous test were due to variations in the geometry or mechanical properties of the dielectric material, the dielectric material was replaced. Subsequent testing showed similar results as with the original dielectric material.

The knee implant was rotated 180° in the gait simulator, to determine if unequal loads were being applied by the gait simulator. The new orientation of the sensors is shown below in Figure 28. Unfortunately, the results from this test were similar to those of Figure 27, which indicates the gait simulator is not causing the difference in sensor readings.

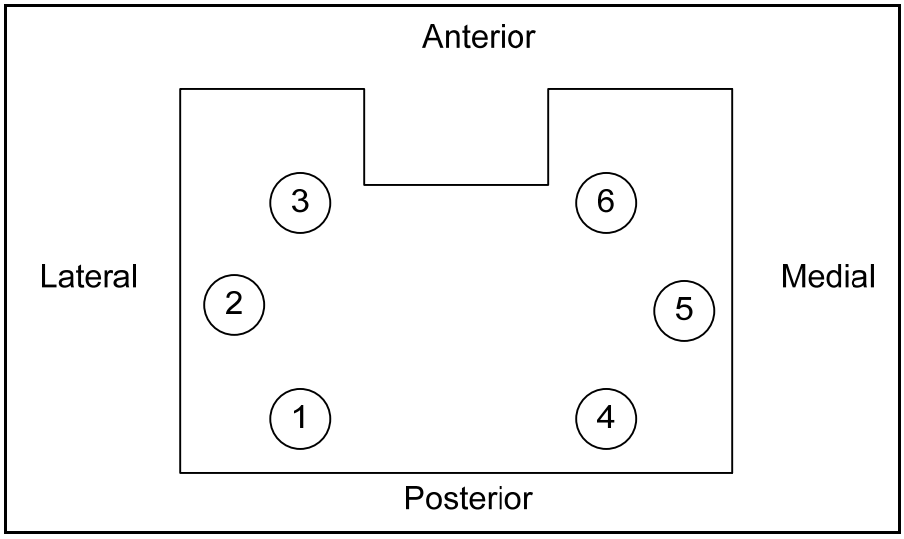

Figure 29 - Layout of capacitive sensors in gait simulator when rotated 180°

By assuming that the load applied to each sensor was equal, the sensors can be calibrated with the previously measured data. To calibrate the sensors, the data from the load cell and capacitive sensors was superimposed and linear scale factors were applied to the sensor measurements until the two graphs were aligned. The resulting graphs are shown below in Figure 29 through Figure 34. The previous assumption was made only to show the potential measurement output of the instrumented tibial tray; future testing will be required to actually measure the forces applied to each sensor to develop more accurate calibration data.

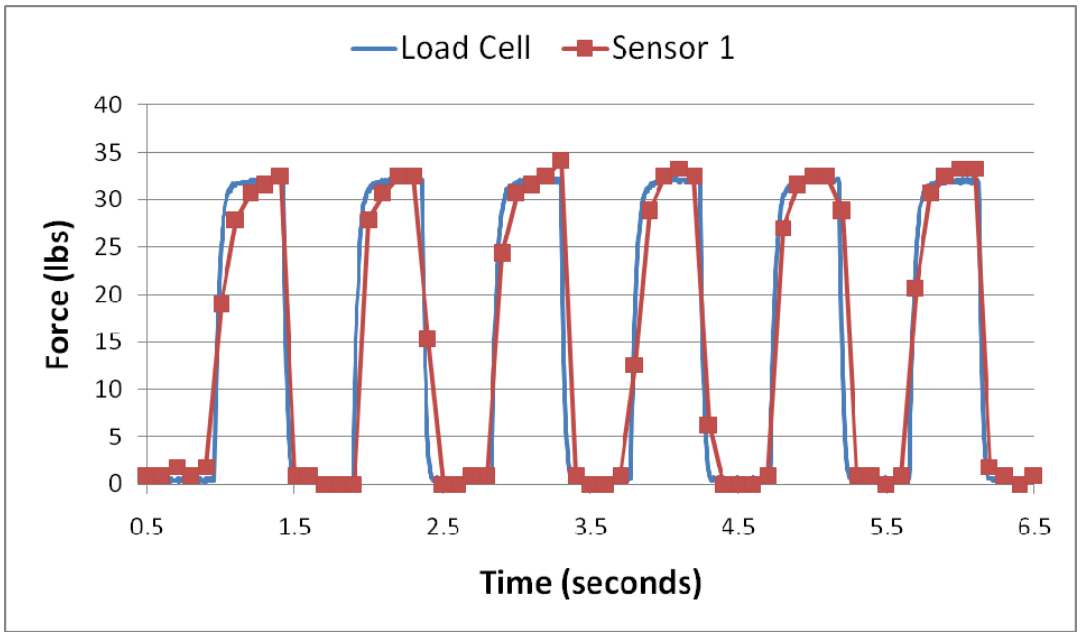

Figure 30 – Force measurements for sensor # 1, after calibration completed

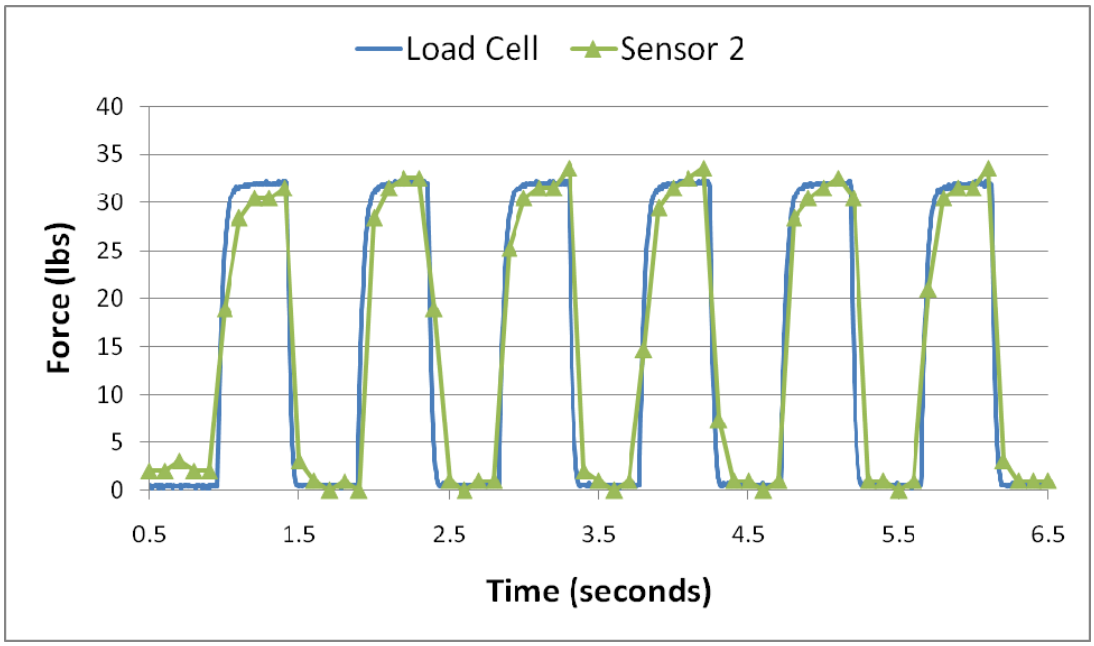

Figure 31 – Force measurements for sensor # 2, after calibration completed

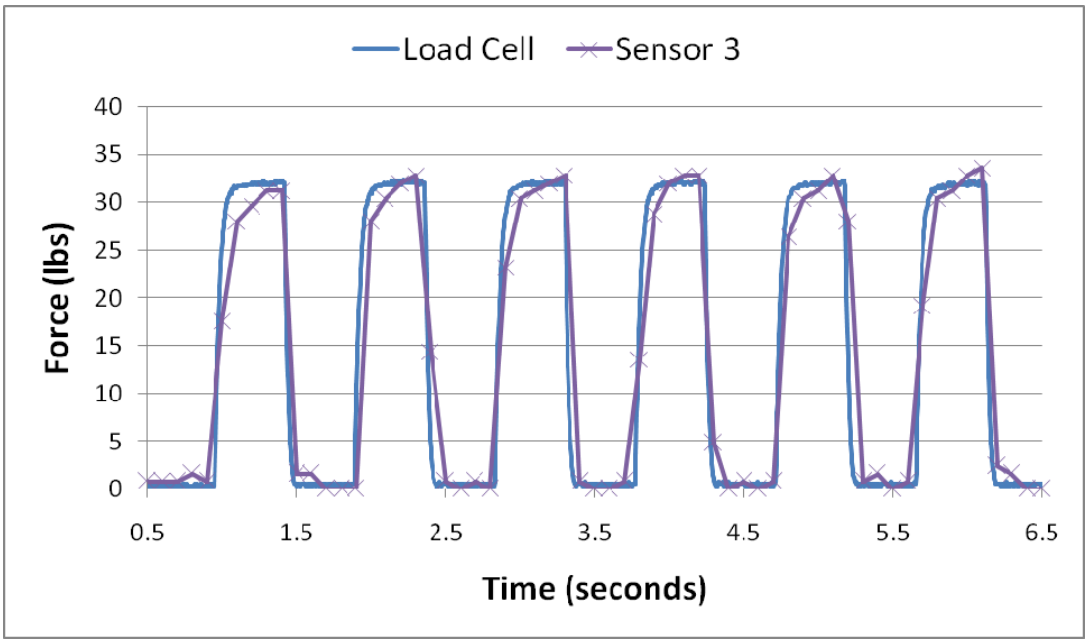

Figure 32 – Force measurements for sensor # 3, after calibration completed

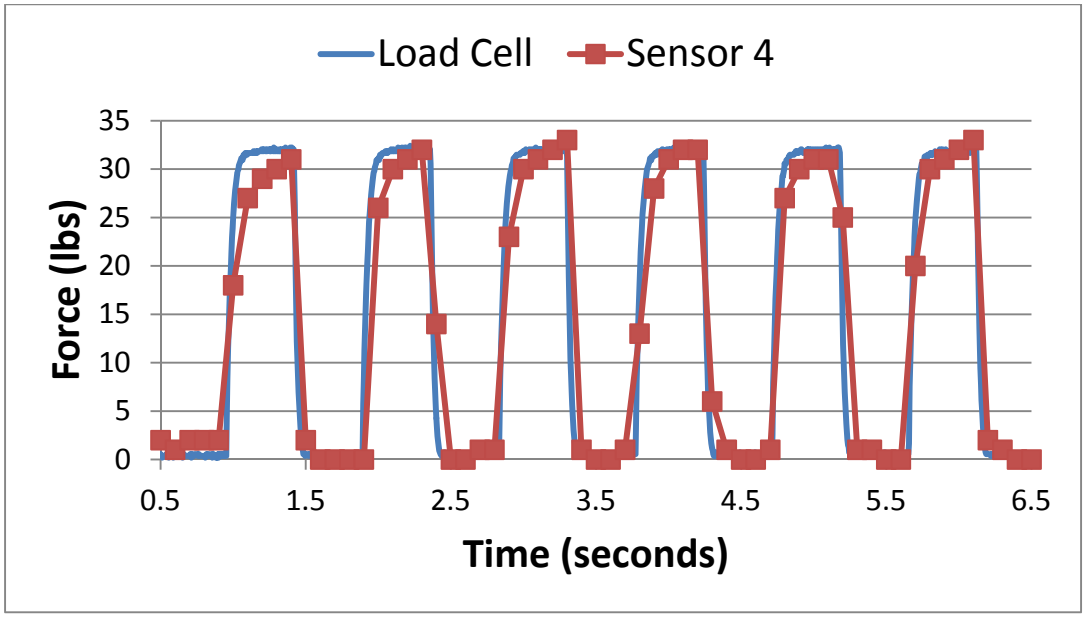

Figure 33 – Force measurements for sensor # 4, after calibration completed

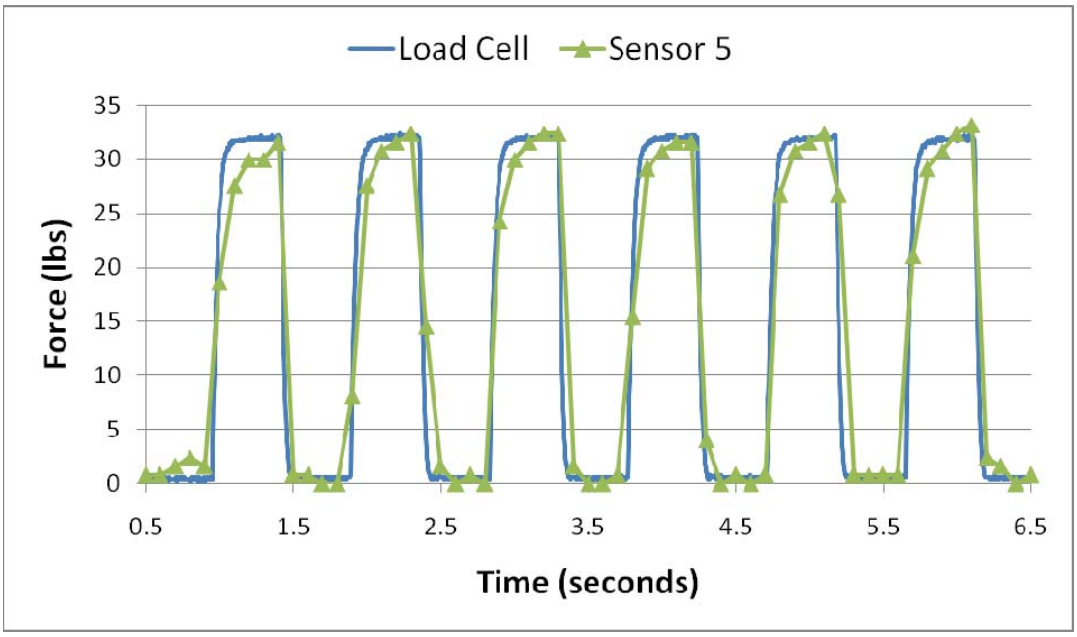

Figure 34 – Force measurements for sensor # 5, after calibration completed

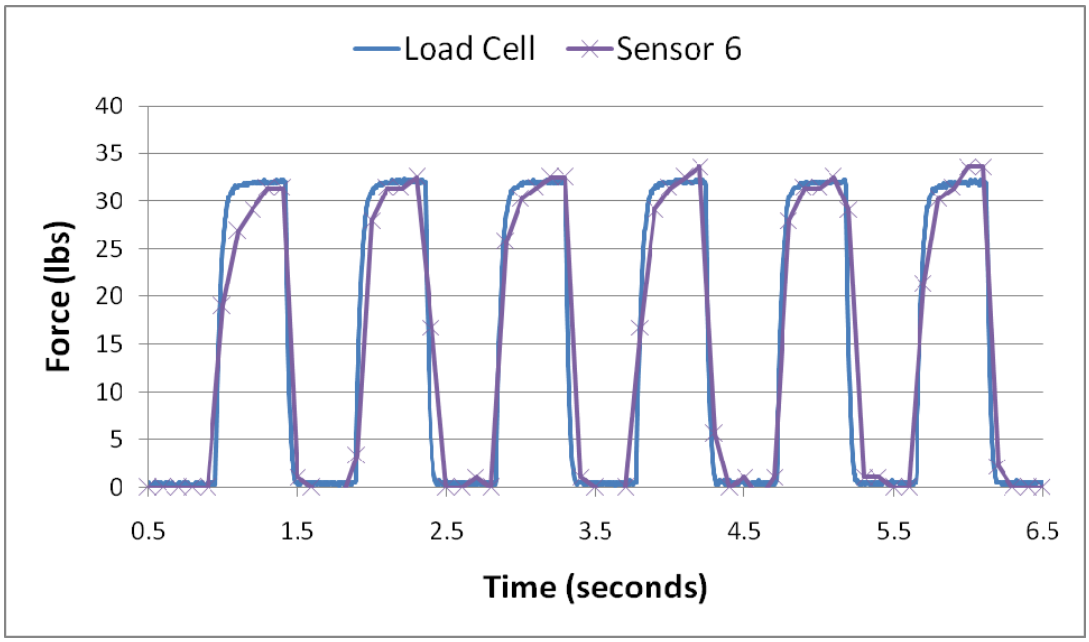

Figure 35 – Force measurements for sensor # 6, after calibration completed

7.4 System Power Consumption

Energy harvesting data reported in Table 4 showed that the storage capacitor could be fully charged in about 23 cycles with a 188 lb load. Now the power consumption of the

system must be measured to determine how quickly the storage capacitor will be drained when measuring the sensors and transmitting data

7.4.1 *Power Consumption while Measuring Sensors*

To understand the power consumption when specifically measuring the sensors, the software code that provided wireless data transmission was removed and the CC430 was reprogrammed. The voltage across the storage capacitors was monitored with an Agilent TDS2022 oscilloscope. Figure 35 below shows the capacitor voltage when the system is strictly measuring the sensors. A switch that connected the CC430 to the storage capacitor was closed about 4 seconds into the data acquisition.

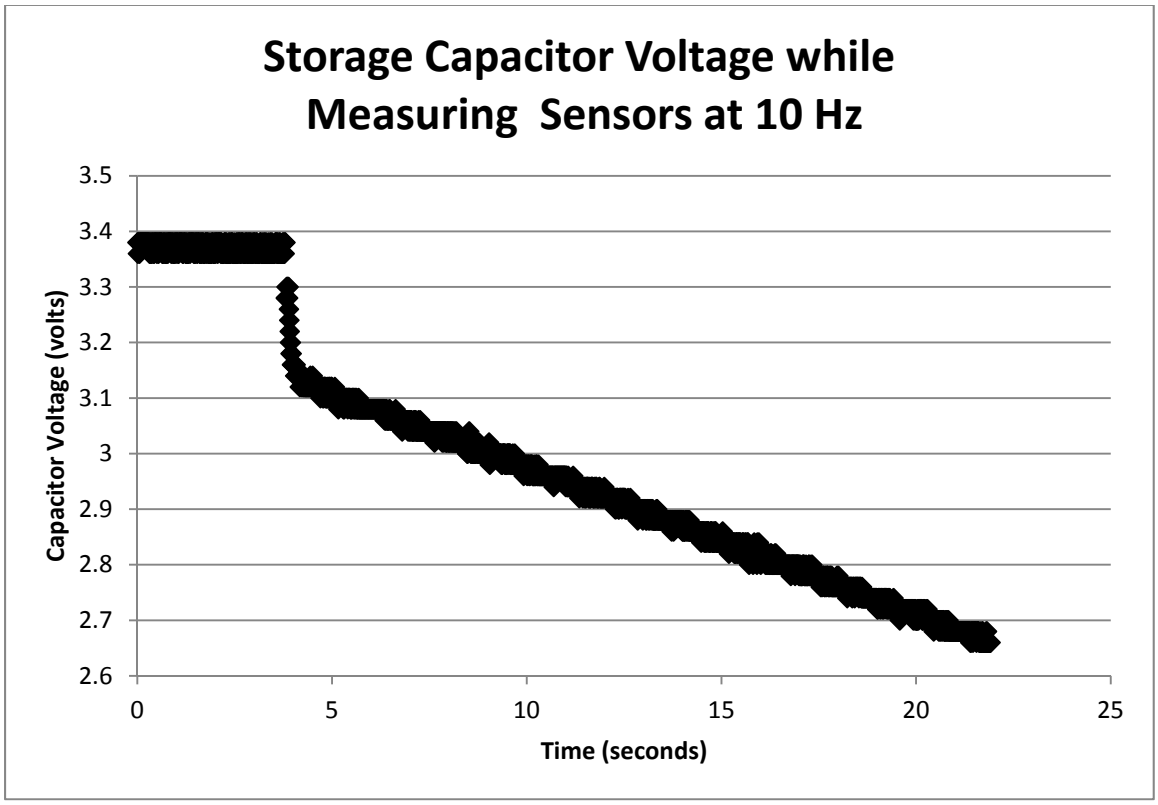

Figure 36 – Storage capacitor voltage while measuring Sensors at 10 Hz

From the graph above, there appear to be two unique regions of power consumption: the initial transient near 4 seconds when the switch was closed and the linear region, after the initial transient, that extends out to t=21.9 sec. The initial transient is due to the CC430 initializing and allowing the clock frequency to stabilize. The linear region after the

initial transient is when the CC430 was actually measuring the sensors. By comparing the stored energy in the storage capacitor before and after the linear region and dividing by the difference in time, the average power while measuring the sensors can be calculated as shown below.

$$P = \frac{\left(\frac{1}{2}\right) \cdot C \cdot (V_2^2 - V_1^2)}{t_2 - t_1} = \frac{\left(\frac{1}{2}\right) \cdot 0.002 \cdot (2.66^2 - 3.14^2)}{21.9 - 4.1} = -0.16mW$$

The measured power consumption is significantly different from the theoretical calculation performed in section 4.2.1.3 , which predicted the power consumption to be -0.02mW. This difference is partially due to the software filtering algorithm, the algorithm to manage the sampling rate of the sensors, and inefficiencies in the software code. By accounting for the first two factors, the theoretical power consumption would increase to -0.05mW.

By comparing the power consumption shown above and the power harvested in Table 4, it becomes apparent that the PEHS will adequately power sensor measurements at 10 Hz when the input force is greater than 110 lbs. Since forces in the knee often exceed 200% of BW while walking on level ground, the PEHS will be in a power-positive situation for patients heavier than 55 lbs, which is almost guaranteed for adult patients. To compensate for the energy lost from the storage capacitor while measuring the sensors, the patient will need to take a few steps during the force measurement process. The specific number of steps depends on the input force. If the force on the piezoelectric transducer is 316 lbs, the patient needs to take approximately two steps. If the force on the piezoelectric transducer is 188 lbs, the patient needs to take approximately four steps

7.4.2 *Power Consumption while Transmitting Data*

The previous section showed very promising results for power consumption while measuring the sensors and storing the data. Now testing must be completed to verify the system can transmit all ten seconds of data for the six sensors.

The voltage across the storage capacitors was monitored with an Agilent TDS2022 oscilloscope. Figure 36 below shows the capacitor voltage when the system is strictly transmitting data.

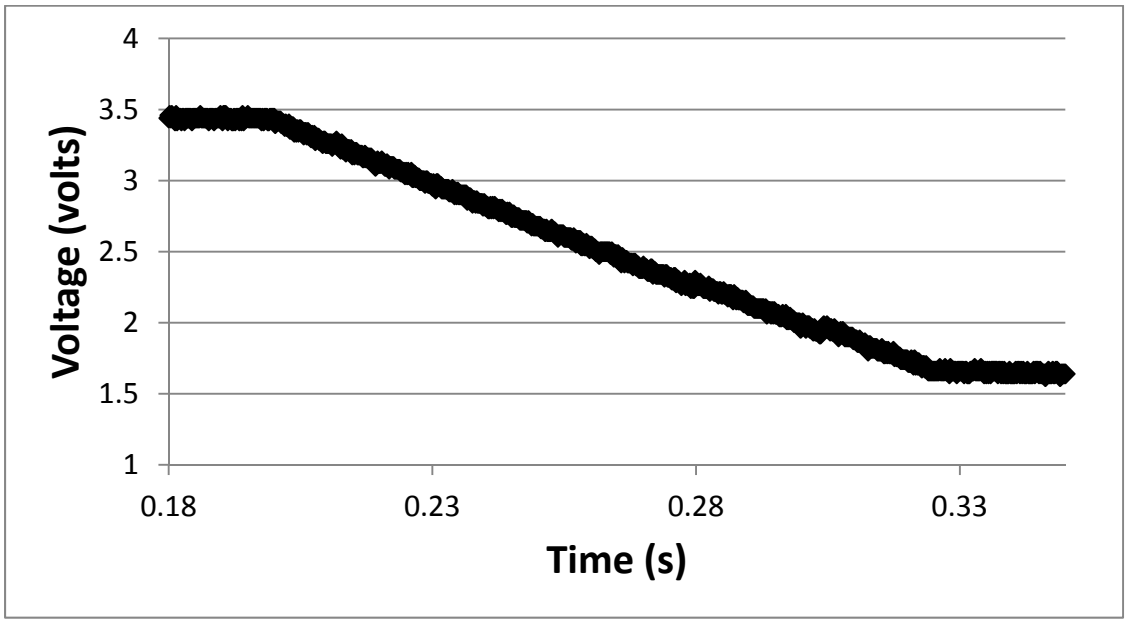

Figure 37 – Storage capacitor voltage while transmitting data

By comparing the stored energy in the storage capacitor before and after the linear region and dividing by the difference in time, the average power while transmitting data can be calculated as shown below.

$$P = \frac{\left(\frac{1}{2}\right) \cdot C \cdot (V_2^2 - V_1^2)}{t_2 - t_1} = \frac{\left(\frac{1}{2}\right) \cdot 0.002 \cdot (1.66^2 - 3.42^2)}{0.324 - 0.201} = -72.8\, mW$$

The measured power consumption is slightly different than the theoretical power consumption calculated in section 5.3. This difference can likely be attributed to higher current consumption than was specified in the CC430 data sheet.

To transmit all ten seconds of data, the storage capacitor should be fully charged before data transmission is initiated. If the previously described process was followed of pre-charging the storage capacitor and auxiliary charging during sensor measurement, the storage capacitor will be fully charged and the data will be successfully transmitted.

Chapter 8 – Conclusions and Future Research

8.1 Summary and Conclusions

The research presented in this thesis attempted to create an instrumented tibial tray capable of measuring loads within the knee and transmitting the resultant data while harvesting energy with an integrated piezoelectric transducer.

A design capable of meeting the performance requirements for the capacitive force sensors was not found. Despite this finding, a set of sensors was designed that could meet some to f the requirements and would help demonstrate the concept. The capacitance of the prototype sensors varied with applied force as was intended; however, the calibration settings for the sensors changed with continued testing, indicating that the sensors had issues with repeatability. The poor repeatability of the sensors is likely caused by the nominal thickness of the compliant material changing due to yielding of the compliant material. Another potential reason for the poor repeatability may be due to differences in the stress-strain response of the compliant material caused by the Mullin's effect.

The performance of the piezoelectric energy harvesting system did not show the expected trend with respect to applied force; but nonetheless, the system demonstrated good performance by quickly charging the storage capacitors, even for loads much less than would be expected in a typical application. The power consumption of the device was so low while measuring the force sensors that the system could collect 45 seconds of data without needing to harvest energy. On the contrary, RF data transmission had high power requirements and turned out to be the limiting factor in how much data could be collected in a single sequence and correspondingly transmitted. To power the force measurement system for ten seconds and to transmit all of the data, the piezoelectric energy harvesting system must be pre-charged by a minimum of 11 steps with a force of 316 lbs and a minimum of two steps must be taken during the force measurement process. This result shows that with a reasonable level of patient activity, the energy

harvesting system can provide sufficient power output to meet the demands of the instrumented tibial tray.

8.2 Future Research

The following are some potential research opportunities that could improve the aforementioned instrumented tibial tray.

- Since the performance of the PEHS did not follow the relationship that was theoretically predicted, and consequently less than was expected, there exists an opportunity to increase the performance of the PEHS. By increasing the performance of the PEHS, several possibilities exist for system improvement: strain gages may become viable, higher sampling rate on the force sensors, and less time required to charge the storage capacitors before the sensors can be measured.
- The deflection of and load transfer through the polyethylene plate and ground plate should be better understood. Ideally, these plates should be designed such that the deflections do not significantly affect the resultant forces measured by the sensors.
- The current capacitive force sensors are designed such that they cannot be individually calibrated, which is a result of using a common ground plate for the sensors. If capacitive sensors are used in the future, a method to calibrate each sensor individually should be investigated.
- The primary limitation for sensor sampling rate and measurement time was the power requirement to transmit the data. To alleviate this issue, a small rechargeable battery could be included to help buffer the system during high load conditions, i.e., while transmitting data.
- A method should be developed to turn the system ON and OFF when implanted in the body. Some options include a magnetic reed switch or duplex RF communication.
- An alternative method to measure the sensor capacitance should be examined. There exist commercially-available capacitance measuring components that have

measurements resolutions in the attofarad range, which could make one of the previously discussed sensor concepts viable.

- The effect of humidity on sensor capacitance needs to be examined.
- Capacitive force sensors are not an established technology, potentially for some of the reasons identified in this paper. A more established force sensor technology should be investigated for this application, such as: piezoresistive sensors, load cells, and strain gages. Load cells and strain gages have already been proven to be effective in similar applications, but the concern is in fitting these sensors into the proposed system and maintaining low power consumption.

Works Cited

ACL Solutions. (n.d.). *Anatomy of the Knee*. Retrieved September 17, 2011, from ACL Solutions: http://www.aclsolutions.com/anatomy.php

Bashirullah, R. (2010). Wireless Implants. *Microwave Magazine, IEEE* , S14-S23.

Bergmann, G., Graichen, F., Rohlmann, A., Westerhoff, P., B. Heinlein, A. B., & Ehrig, a. R. (2008). Design and Calibration of Load Sensing Orthopaedic Implants. *Journal of Biomechanical Engineering* .

Bozic, K., Kurtz, S., Lau, E., Ong, K., Chiu, V., Vail, T., et al. (2010). The Epidemiology of Revision Total Knee Arthroplasty in the United States. *Clinical Orthopaedics and Related Research* , 45-51.

D'Lima, D. D., Steklov, N., Fregly, B. J., Banks, S. A., & Colwell, C. W. (2008). In vivo contact stresses during activities of daily living after knee arthroplasty. *Journal of Orthopaedic Research* , 1549-1555.

D'Lima, D. D., Townsend, C. P., Arms, S. W., Morris, B. A., & Jr, C. W. (2005). An implantable telemetry device to measure intra-articular tibial forces. *Journal of Biomechanics* , 299-304.

Godest, A. C., Beaugonin, M., Haug, E., Taylor, M., & Gregson, P. J. (2002). Simulation of a knee joint replacement during a gait cycle using explicit finite element analysis. *Journal of Biomechanics* , Pages 267-275.

Graichen, F., Arnold, R., Rohlmann, A., & Bergmann, G. (2007). Implantable 9-Channel Telemetry System for In Vivo Load Measurements With Orthopedic Implants. *Biomedical Engineering, IEEE Transactions on* , 253-261.

Guan, M., & Liao, W. (2007). Characteristics of Energy Storage Devices in Piezoelectric Energy Harvesting Systems. *Journal of Intelligent Material Systems and Structures* , 671-680.

Heinlein, B., Graichen, F., Bender, A., Rohlmann, A., & Bergmann, G. (2007). Design, calibration and pre-clinical testing of an instrumented tibial tray. *Journal of Biomechanics* , S4-S10.

Heinlein, B., Kutzner, I., Graichen, F., Bender, A., Rohlmann, A., Halder, A. M., et al. (2009). ESB clinical biomechanics award 2008: Complete data of total knee

replacement loading for level walking and stair climbing measured in vivo with a follow-up of 6-10 months. *Clinical Biomechanics* , 315-326.

Hospital for Special Surgery Website, HSS.edu. (2010, June 14). *Hospital for Special Surgery Website, HSS.edu*. Retrieved September 17, 2011, from http://www.hss.edu/images/articles/tnr-4.jpg

Kaufman, K. R., Kovacevic, N., Irby, S. E., & Colwell, C. W. (1996). Instrumented implant for measuring tibiofemoral forces. *Journal of Biomechanics* , 667-671.

Kurtz, S., Ong, K., Edmund, L., Mowat, F., & Halpern, M. (2007). Projections of Primary and Revision Hip and Knee Arthroplasty in the United States from 2005 to 2030. *The Journal of Bone and Joint Surgery* , 780-785.

Kutzner, I., Heinlein, B., Graichen, F., Bender, A., Rohlmann, A., Halder, A., et al. (2010). Loading of the knee joint during activities of daily living measured in vivo in five subjects. *Journal of Biomechanics* , 2164-2173.

McCrum, N., Buckley, C., & Bucknall, C. (1997). *Principles of Polymer Engineering, Second Edition.* New York: Oxford University Press.

Morrison, J. (1970). The mechanics of the knee joint in relation to normal walking. *Journal of Biomechanics* , 51-61.

Mündermann, A., Dyrby, C. O., D'Lima, D. D., Colwell, C. W., & Andriacchi, T. P. (2008). In vivo knee loading characteristics during activities of daily living as measured by an instrumented total knee replacement. *Journal of Orthopaedic Research* , 1167-1172.

NIH Consensus Development Conference on Total Knee Replacement. (2003, December 8-10). Retrieved from National Institutes of Health: http://consensus.nih.gov/2003/2003TotalKneeReplacement117html.htm

Ong, K., Lau, E., Suggs, J., Kurtz, S., & Manley, M. (2010). Risk of Subsequent Revision after Primary and Revision Total Joint Arthroplasty. *Clinical Orthopaedics and Related Research* , 3070-3076.

Orthoload. (2011, August 4). *k1l_110108_1_80p*. Retrieved September 17, 2011, from Orthoload: http://www.OrthoLoad.com

Ottman, G., Hofmann, H., Bhatt, A., & Lesieutre, G. (2002). Adaptive Piezoelectric Energy Harvesting Circuit for Wireless Remote Power Supply. *Power Electronics, IEEE Transactions on* , 669- 676.

Park, C. (2001). ON the Circuit Model of Piezoceramics. *Journal of Intelligent Material Systems and Structures* , 515-522.

Piezo Systems Inc. (n.d.). *Introduction to Piezo Transducers*. Retrieved August 31, 2011, from Piezo Systems Inc: http://www.piezo.com/tech2intropiezotrans.html

Sigma Fixed Bearing Knee System. (2010). Retrieved from Depuy: http://www.depuy.com/sites/default/files/products/images/Sm-Sigma-FB.jpg

Simon H Palmer, M., & Mervyn J Cross. (2009, April 14). *Total Knee Arthroplasty*. Retrieved from eMedicine: http://emedicine.medscape.com/article/1250275-overview

Tabesh, A., & Frechette, L. (2010). A Low-Power Stand-Alone Adaptive Circuit for Harvesting Energy From a Piezoelectric Micropower Generator,. *Industrial Electronics, IEEE Transactions on* , 840-849.

Texas Instruments. (2007, October). SLAA363A - PCB-Based Capacitive Touch Sensing with MSP430.

Texas Instruments. (2010, November). SLAS554E - CC430F613x Data Sheet.

Tokuhara, Y., Kadoya, Y., Nakagawa, S., Kobayashi, A., & Takaoka, K. (2004). The flexion gap in normal knees: AN MRI STUDY. *Journal of Bone and Joint Surgery* , 1133-1136.

Vijayaraghavan, K., & Rajamani, R. (2010). Ultra-Low Power Control System for Maximal Energy Harvesting From Short Duration Vibrations. *Control Systems Technology, IEEE Transactions on* , 252-266.

Appendix A

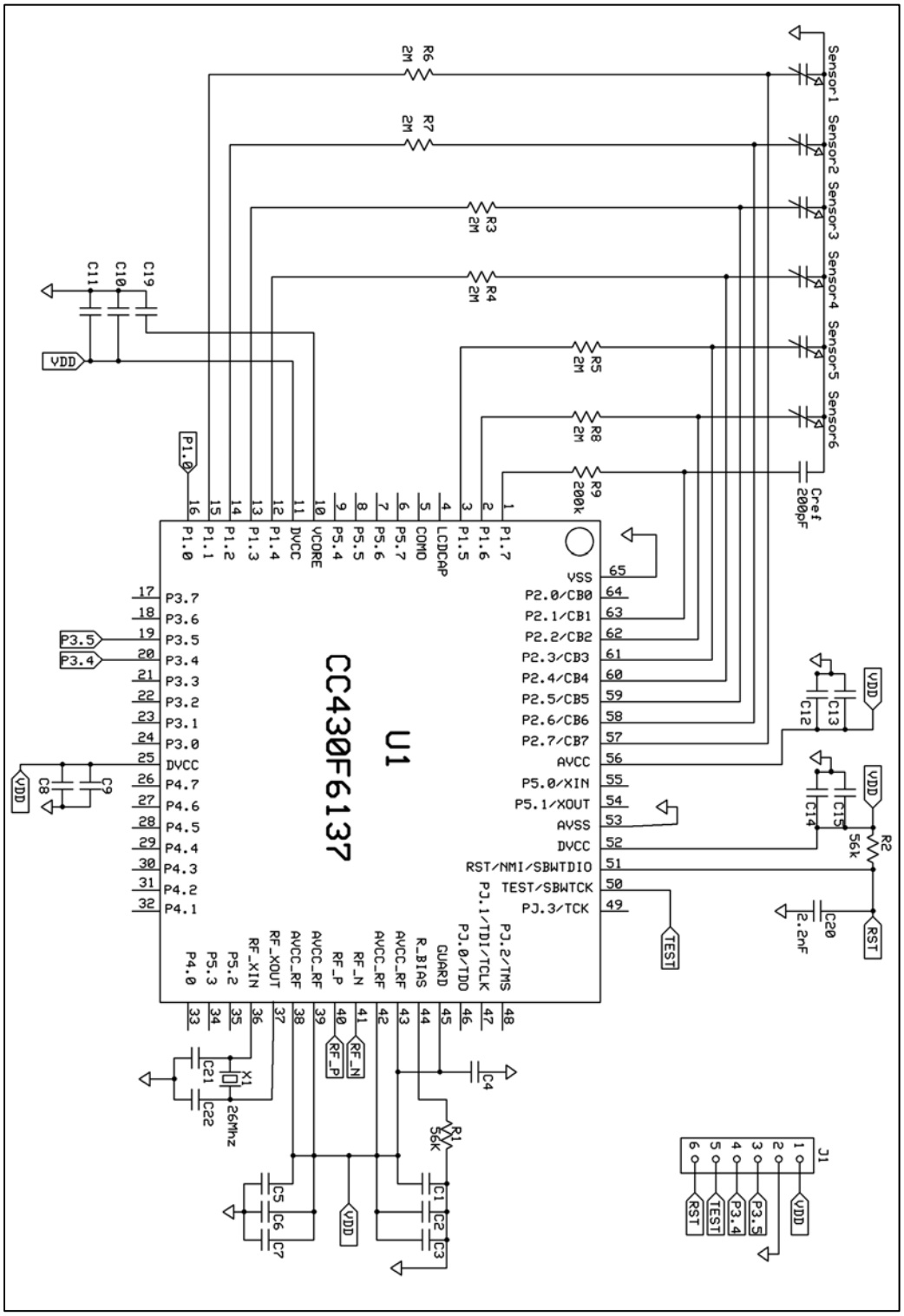

Figure 38 – Page 1 of schematic for electrical circuit

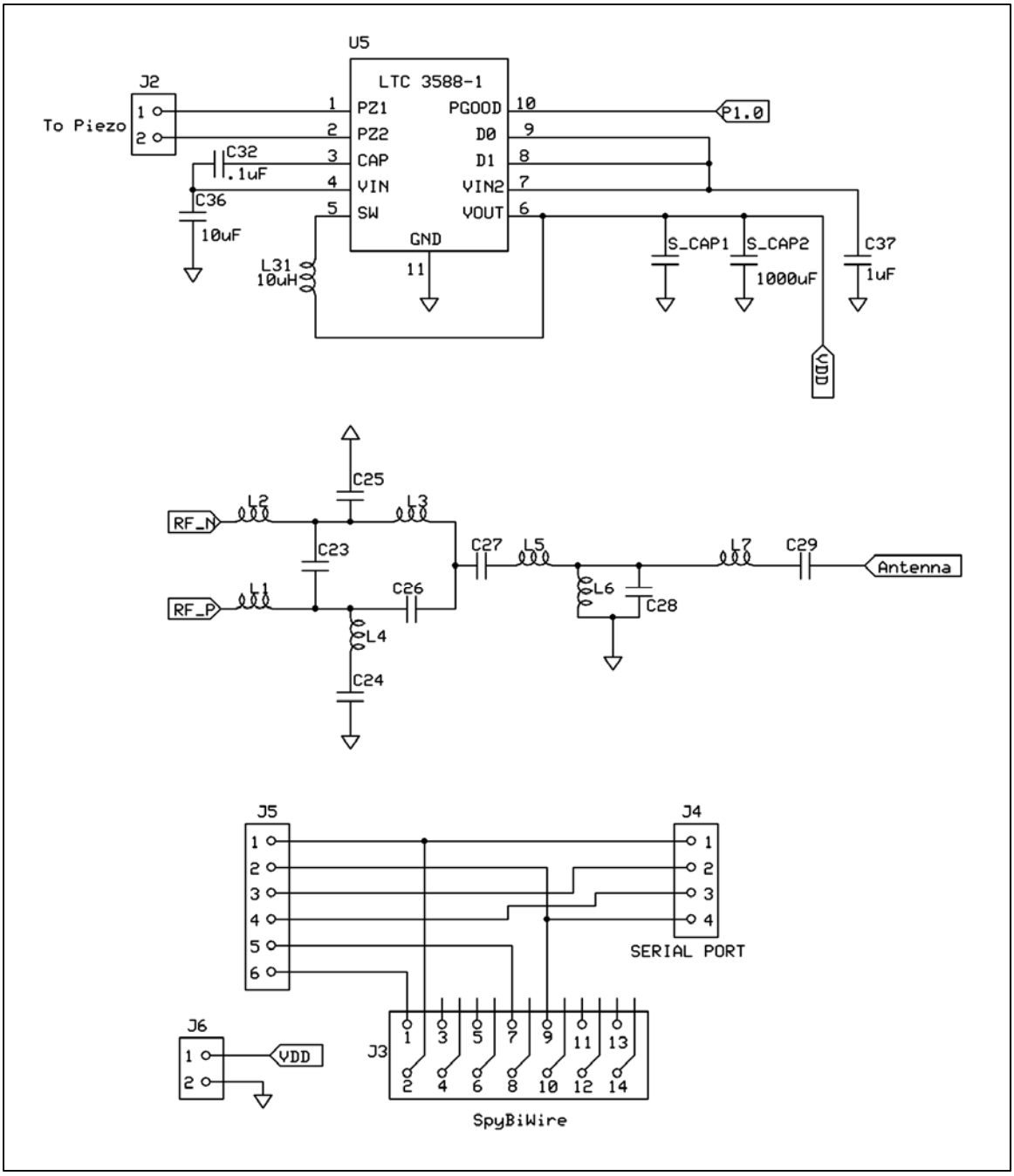

Figure 39 – Page 2 of schematic for electrical circuit

Appendix B

Below are pictures of the final device.

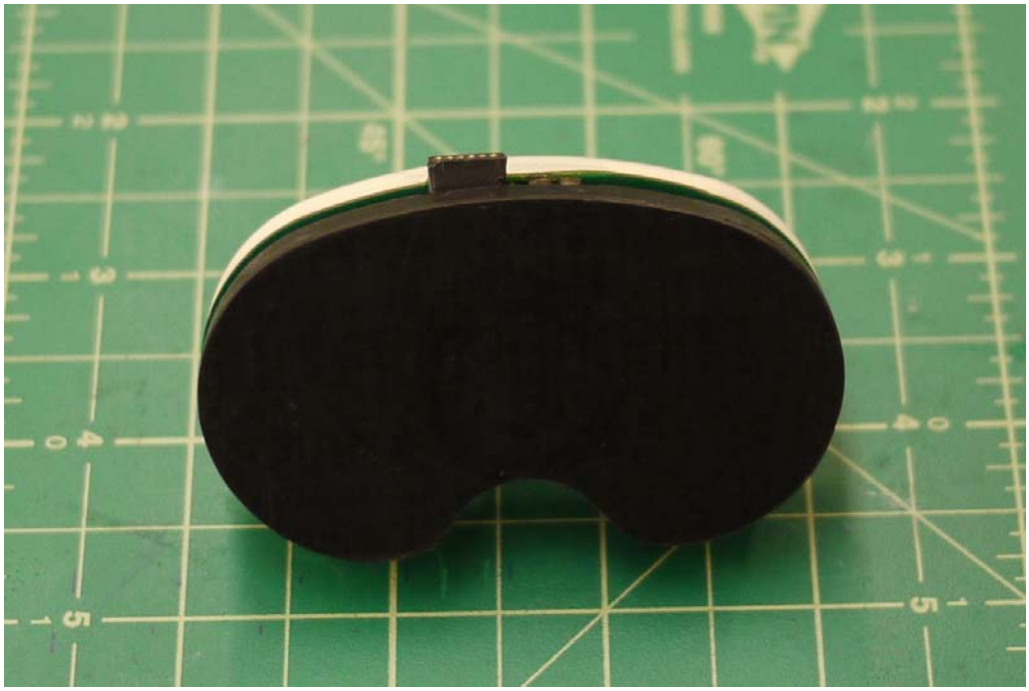

Figure 40 – Front view of final device

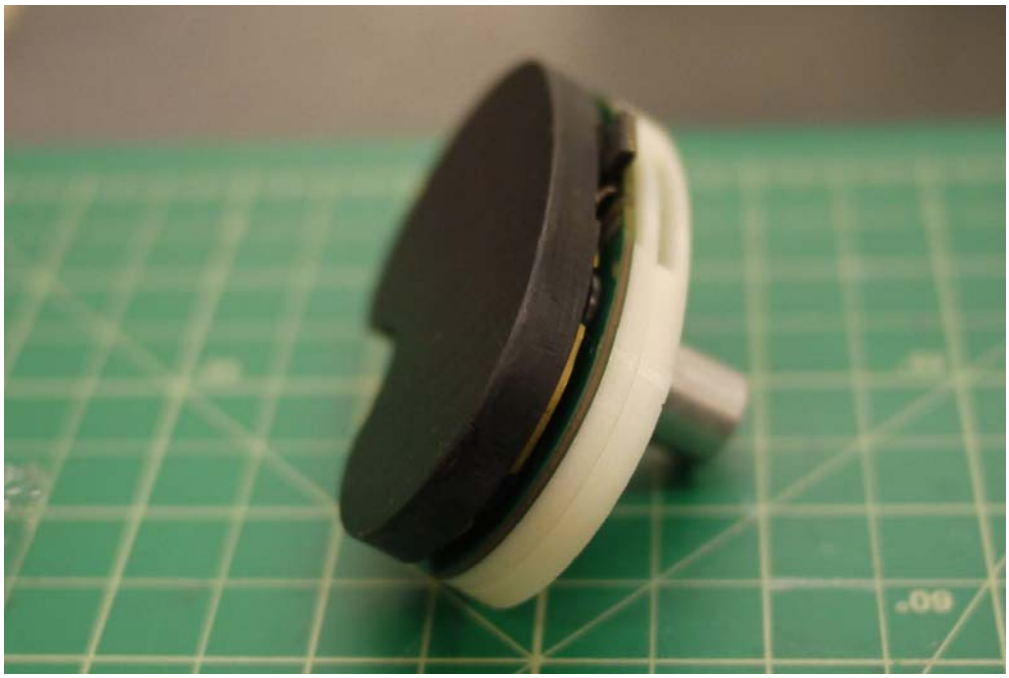

Figure 41 – Side view of final device

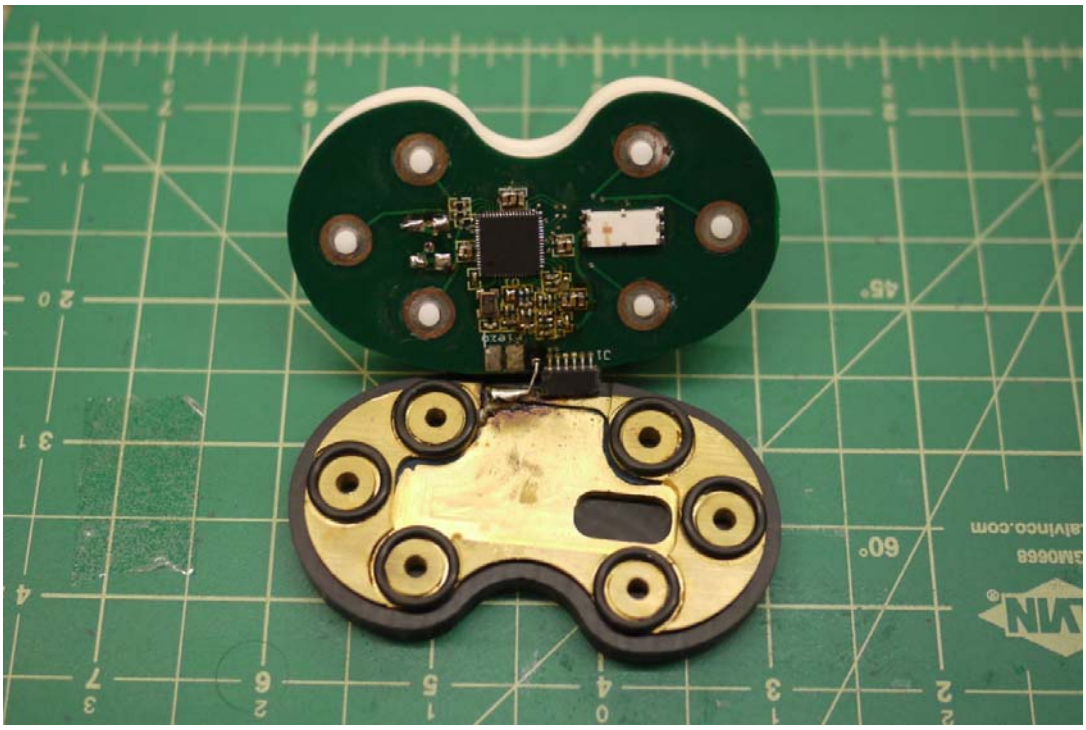

Figure 42 – Picture showing circuit board, ground plate, and compliant material for sensors